https://doi.org/10.5194/egusphere-2023-817
Preprint. Discussion started: 4 May 2023

Spatiotemporal variations in terrestrial biospheric CO_2 fluxes of India derived from MODIS, OCO-2 and TROPOMI satellite observations and a diagnostic terrestrial vegetation model

Aparnna Ravi [1,2], Dhanyalekshmi Pillai [1,2], Christoph Gerbig [3], Stephen Sitch[4], Sönke Zaehle[3], Vishnu Thilakan[1,2], and Chandra Sekhar Jha [5]

Corresponding author: Dhanyalekshmi Pillai[1,2], dhanya@iiserb.ac.in

[1]Indian Institute of Science Education and Research Bhopal (IISERB), India,

[2]Max Planck Partner Group at IISERB, Bhopal, India,

[3]Max-Planck Institute of Biogeochemistry, Jena, Germany,

[4]University of Exeter, Exeter EX4 4QF, UK,

[5]National Remote Sensing Centre (ISRO), Balanagar, Hyderabad, India.

https://doi.org/10.5194/egusphere-2023-817
Preprint. Discussion started: 4 May 2023

Abstract

Accurate quantification of regional terrestrial fluxes is essential for improving our knowledge of the carbon sequestration potential of ecosystems, ecosystem functioning, and emission reduction demand in the context of climate change mitigation. However, the quantification is challenging owing to methodological and observational constraints, especially for regions with severe gaps in the ground-based observational network, like India. This study examines the potential of recent satellite missions, such as TROPOMI and OCO-2 providing retrievals of Solar-Induced chlorophyll Fluorescence (SIF) to improve terrestrial biosphere CO_2 flux estimates over India. Here, we present high-resolution estimates of Gross Primary Productivity (GPP) and Net Ecosystem Exchange (NEE) over India on a 0.1°×0.1° grid at a temporal resolution of 1 hour from 2012 to 2020. These products can be used for various applications such as those related to carbon cycle (e.g., inverse modelling of CO_2), benchmarking terrestrial biosphere models over the region, and understanding ecosystem responses to climate change. We follow a satellite-based diagnostic data-driven approach using a biosphere model, namely the Vegetation Photosynthesis and Respiration Model (VPRM) simulating both GPP and NEE, based on light use efficiency and satellite observations of the near-infrared radiance of vegetation (NIRv). We calibrate the standard VPRM GPP estimates using SIF-GPP relationship and investigate the model performance by comparing the simulations with eddy-covariance flux tower measurements. Our best model predictions are with a mean bias error (MBE) = 2.4 µmol m^{-2} s^{-1}, root mean squared error (RMSE) = 3.8 µmol m^{-2} s^{-1} and squared correlation coefficient (R^2) = 0.56 when evaluating with observations at a monthly scale over the period from 2012 to 2018. The observed seasonal anomalies in NEE and GPP range from -4.9 to 8.0 µmol m^{-2} s^{-1} and -7.0 to 17.0 µmol m^{-2} s^{-1}, respectively, and are well captured by our model. The model simulations are highly correlated with observations during 2018, the only common year when both EC and SIF observations are available,

https://doi.org/10.5194/egusphere-2023-817
Preprint. Discussion started: 4 May 2023

with R^2 values of 0.68 and 0.74 for NEE and GPP, respectively. Incorporating the SIF signals in the vegetation model improves model performance in capturing the seasonality and magnitudes of GPP, thereby improving the estimates of NEE. We show the influence of soil temperature and soil moisture on ecosystem respiration and refined the VPRM's ecosystem respiration calculation to better constrain the fluxes, resulting in simulations closer to the observations. Ecosystem respiration fluxes are less well constrained than ecosystem productivity fluxes due to the limited observations. Based on satellite observations and the refined model, the annual NEE and GPP estimates range from -0.38 Pg C yr^{-1} to -0.53 Pg C yr^{-1} (land C sink) and 3.39 Pg C yr^{-1} to 3.88 Pg C yr^{-1}, respectively over India for the years from 2012 to 2020. The biospheric flux distribution over the region is found to be associated with ecosystem heterogeneity, and variations in precipitation, and soil characteristics at a regional scale. Overall, our results show that the satellite-based SIF data products can potentially inform the ecosystem-scale vegetation responses across biomes over India. Future improvements in the terrestrial biosphere CO_2 flux estimates over India can be attained through the carbon cycle data assimilation with the availability of both flux and mixing ratio observations of CO_2.

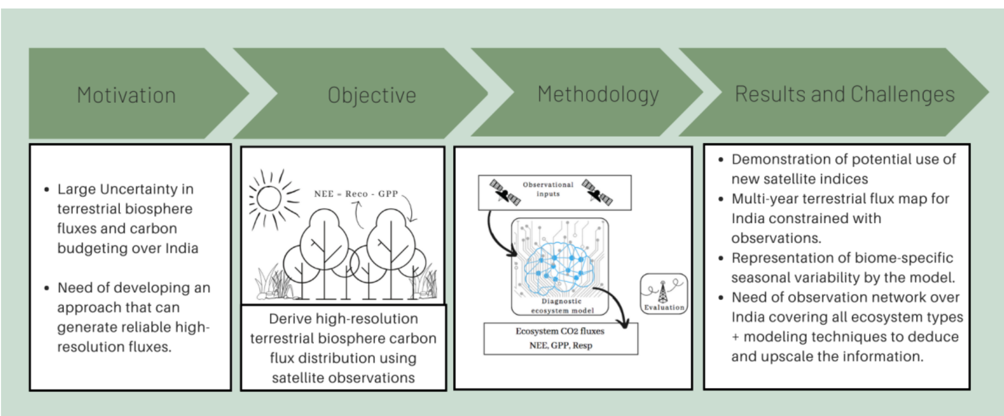

https://doi.org/10.5194/egusphere-2023-817
Preprint. Discussion started: 4 May 2023

1. Introduction

The terrestrial biosphere is the largest sink of atmospheric CO_2. Globally, the net sequestration capacity of the terrestrial biosphere is ~3 Pg C yr^{-1}, corresponding to approximately a quarter of the global annual CO_2 emissions (Friedlingstein et al., 2022). Because of the vital role of the terrestrial biosphere in assimilating and exchanging atmospheric CO_2 with reservoirs, global initiatives to reduce greenhouse gas (GHG) emissions have included the active management of the terrestrial biosphere as a complementary measure for curtailing the emissions (Framework Convention on Climate Change available at http://www.unfccc.de/resource/cop3.htm) in the context of current and future climate.

However, the accurate estimation of terrestrial biosphere-atmosphere exchange fluxes at the scales relevant for climate change mitigation, which is well beyond the scale of single site observations, is still challenging. Major terrestrial fluxes, includes gross fluxes, Gross Primary Production (GPP), and Ecosystem respiration (R_{eco}), and their net, Net Ecosystem Exchange (NEE=R_{eco}-GPP), show considerable spatiotemporal variability owing to the differences in vegetation class and age, as well as in ecosystem response to the climate, geographic conditions, and other location-specific environmental factors (van der Meer et al., 2002). Terrestrial biosphere models can simulate these fluxes at different spatial and temporal scales over the globe (Peylin et al., 2013; Sitch et al., 2008, 2015; Thompson et al., 2016), however these model estimates often suffer from multiple sources of uncertainties, which include: the uneven distribution of eddy covariance flux tower observations worldwide for model validation or calibration, incomplete representation of vital processes in the model (e.g., drought-related mortality), and the insufficient understanding of how environmental factors affect atmosphere-biosphere carbon exchange. For example, the models are constrained with few observations over the Indian subcontinent, resulting in low confidence in the estimates of fluxes over India despite its important role in the global carbon

https://doi.org/10.5194/egusphere-2023-817
Preprint. Discussion started: 4 May 2023

budget. The annual NEE estimates of India from previous studies range from 0 to -0.37 Pg C yr^{-1} (Nayak et al., 2015; Patra et al., 2011; Rao et al., 2019). The spread among twelve vegetation models in estimating the annual NEE of India for 2017 is 0.2 Pg C yr^{-1}, which is close to the magnitude of the Indian terrestrial sink estimation itself (Sitch et al., 2015), leaving the country's carbon flux estimates primarily uncertain.

Atmospheric CO_2 measurements, including those from satellite instruments, can be utilised in an atmospheric inversion modelling framework to evaluate and improve the terrestrial biosphere estimates of India. Simultaneously, prior estimates of biospheric fluxes with reasonable spatiotemporal distributions are advantageous for the atmospheric inverse modelling to obtain the optimal solution to the inverse problem with an improved confidence level (Michalak, 2004; Rayner et al., 1999). The choice of prior and their spatiotemporal structures can be critical when solving an ill-posed inverse problem (Rodgers, 2000). Previous studies have relied on the Light Use Efficiency (LUE) model CASA (Carnegie Ames Stanford Approach; Gamon et al. (1995)) and TRENDY model ensembles (Sitch et al., 2015) for estimating the spatiotemporal patterns of biospheric CO_2 fluxes over southeast Asia covering India (Cervarich et al., 2016; Patra et al., 2011; Peylin et al., 2013) and for India specifically (Goroshi et al., 2014; Nayak et al., 2010, 2013). However, these models are employed at coarse resolution, e.g., $2' \times 2'$ spatial and monthly temporal resolution for CASA, and TRENDY with sub-daily temporal resolution (with output available monthly) and varying spatial resolution with respect to the model, typical 0.5° or above (see Table 3 for further details), with limited model validation against observations over India. This leads to inadequate capturing of the spatiotemporal distribution of fluxes, resulting in varied estimates among studies (Cervarich et al., 2016; Patra et al., 2013; Rao et al., 2019).

https://doi.org/10.5194/egusphere-2023-817
Preprint. Discussion started: 4 May 2023

Recent advancements in satellite instruments, measuring Solar-Induced chlorophyll Fluorescence (SIF) from space can be helpful, especially for the region with severe gaps in ground-based in-situ observations. These satellite-based SIF retrievals, representing re-emitted solar radiation at the long wavelength range (650–850 nm) by the chlorophyll-a pigment, can be utilised to improve the prior estimates of carbon uptake through photosynthesis at regional to global scales (Frankenberg et al., 2011; Gu et al., 2019; Köhler et al., 2018; Li et al., 2018; Smith et al., 2018; Sun et al., 2017; Yu et al., 2019). Since the re-emission process (fluorescence) by chlorophyll is linked to the primary steps in photosynthesis, SIF can be used as the proxy for photosynthesis (Parazoo et al., 2018; Sun et al., 2018; Yu et al., 2019). Only ~2% of the incident solar energy absorbed by green plants is re-emitted by chlorophyll as fluorescence. Thus, SIF retrievals from space need advanced spectrometers with a high spectral resolution and a high Signal-to-Noise Ratio (SNR) due to narrow Fraunhofer lines and weak signals. However, SIF observations are prone to systematic errors which are associated with the strength and extraction range of the signal (Joiner et al., 2016; Köhler et al., 2015; Li et al., 2018). The SIF-GPP relationship can become weak in certain environmental conditions such as drought (e.g., Shekhar et al. (2022) and variable within certain biome based on leaf physiology (e.g., Wu et al. (2022)). The first satellite-based global retrievals of SIF are achieved by the Fourier transform spectrometer (fluorescence spectrum at 755–775 nm) on board the Greenhouse gases Observing SATellite (GOSAT). Other satellite missions that provide SIF retrievals at different spatial and temporal resolutions are GOME-2 (Global Ozone Monitoring Experiment 2; Frankenberg et al. (2011)), OCO-2 (Orbiting Carbon Observatory 2; Sun et al. (2018)), OCO-3 (Orbiting Carbon Observatory 3; Taylor et al. (2020)), and TROPOMI (TROPOspheric Monitoring Instrument; Guanter et al. (2021)).

This study presents high-resolution terrestrial biosphere CO_2 flux estimates over India on a 0.1°×0.1° grid at a temporal resolution of 1 hour for the period from 2012 to 2020. These high-

https://doi.org/10.5194/egusphere-2023-817
Preprint. Discussion started: 4 May 2023

resolution biospheric flux products can be used in the near-future as prior estimates in the inverse data assimilation of CO_2 or can be coupled with high-resolution transport models for understanding the atmospheric CO_2 transport or variability associated with natural fluxes. We follow a diagnostic data-driven approach using a biosphere model based on light-use efficiency and satellite observations of SIF and demonstrate their potential to capture the spatiotemporal variations of biosphere fluxes. The gridded NEE, GPP and R_{eco} are initially generated by utilising the diagnostic satellite-based biosphere model, namely Vegetation Photosynthesis and Respiration Model (VPRM; Mahadevan et al. (2008)). Previously, Thilakan et al. (2022) have generated the VPRM simulations of terrestrial biosphere fluxes (NEE, GPP, and R_{eco}) over the Indian subcontinent at a spatial resolution of 0.1°×0.1° and a temporal resolution of 1 hour using uncalibrated model parameters. These VPRM fields are revised by improving the ecosystem uptake across different biomes using SIF retrievals from OCO-2 and TROPOMI, which provide much finer resolutions and higher data density over the region than those from previous missions (e.g., GOSAT and GOME-2). As we expect a distinct contribution of soil moisture stress in ecosystem respiration signals, we also re-define R_{eco} calculation in the VPRM (originally as a linear function of air temperature) to include the influence of both, soil temperature and soil moisture so that the NEE estimates can be improved. A recent study over the Eastern USA and Canada has also showed improvements in R_{eco} simulations when including the influence of changing foliage, water stress and non-linear dependence of temperature (Gourdji et al., (2022).

Variations in temperature, radiation, and resource availability (e.g., water and soil nutrients) influence plant phenology and ecosystem stress levels, contributing to seasonal anomalies in GPP and NEE. It remains challenging to accurately represent the seasonal dynamic attributes of ecosystem fluxes and simulate their associated variability. In this study, we assess the usefulness of the SIF signals to capture the seasonality and magnitudes of GPP in the model by comparing

https://doi.org/10.5194/egusphere-2023-817
Preprint. Discussion started: 4 May 2023

them with eddy-covariance flux tower measurements from India for the period from 2012 to 2018. We further investigated the influence of environmental factors and processes on modelled respiration at the regional level. We assess the VPRM against estimates from TRENDY model ensemble and Carbon Tracker inversion. By improving the diagnostic biospheric model and generating simulations at a high resolution, comparing the derived flux components from multiple terrestrial models, and evaluating the improved model against observations, we investigate the spatial and temporal variations of biosphere fluxes in different ecosystems over India on seasonal and annual scales.

2. Methods

For deriving improved estimates of terrestrial biosphere CO_2 fluxes across the ecosystem over India: i) we implement and customise the standard VPRM for a domain covering India (5°N to 40°N, 66°E to 100°E, Fig. 1 and Fig. S1) and perform the simulations of NEE, GPP and R_{eco} fluxes (Sect. 2.1); ii) we derive ecosystem-specific linear relations between SIF and GPP using SIF retrievals based on OCO-2 and TROPOMI (detailed in Sect. 2.2); iii) we apply the above satellite-derived information in the VPRM to improve the estimates of the ecosystem uptake (Sect. 2.2); and iv) we further modify the VPRM-derived ecosystem respiration to include the influence of soil temperature and soil moisture specific to vegetation classes (Sect. 2.3).

We compare the standard and improved VPRM simulations with the TRENDY model ensemble and other model simulations (Sect. 2.4) and evaluate the simulations with the flux tower observations (Sect. 2.5). In this section, we also describe the approaches used for overall analyses for assessing the model's performance and deriving the spatiotemporal characteristics of fluxes (Sect. 2.6). An overview of the datasets used in the study is presented in Table 1.

2.1 VPRM model implementation

https://doi.org/10.5194/egusphere-2023-817
Preprint. Discussion started: 4 May 2023

The standard VPRM employs a remote sensing-based scheme to obtain high-resolution estimates of NEE, GPP and R_{eco}, using Enhanced Vegetation Index (EVI) and Land Surface Water Index (LSWI), derived from the Moderate Resolution Imaging Spectroradiometer (MODIS) measurements onboard the NASA's Terra and Aqua satellites. We use the MODIS tiles of the surface reflectance dataset (MOD09A1) on sinusoidal grids at a 500 m spatial resolution with an 8-day interval to generate EVI and LSWI fields. Specifically, we use the red band (band 1), the near-infrared band (band 2), the blue band (band 3) for deriving EVI, and the near-infrared band (band 2) and the shortwave infrared band (band 6) for deriving LSWI. For representing different biomes in VPRM, we use vegetation classification based on SYNMAP (Jung et al., 2006).

In VPRM, NEE for each vegetation class is calculated based on GPP (light-dependent term) and R_{eco} (light-independent term). NEE is assessed based on the sign convention where negative values indicate CO_2 uptake and positive values represent CO_2 release into the atmosphere.

$$NEE = -GPP + R_{eco} \quad (1)$$

$$GPP = \lambda \times P_{scale} \times W_{scale} \times FPAR_{PAV} \times \frac{1}{[1+(SW_{down}/SW_{downo})]} \times SW_{down} \times T_{scale} \quad (2)$$

$$R_{eco} = \alpha \times T_{air} + \beta \quad (3)$$

where λ is the factor representing light use efficiency. $FPAR_{PAV}$ is the fraction of photosynthetically active radiation available to the photosynthetically active part of vegetation which is derived from MODIS EVI. T_{scale}, P_{scale} and W_{scale} are dimensionless scalars representing the sensitivity of plants to changes in temperature, phenology, and water availability, respectively. T_{scale} is derived using ecosystem-specific temperature as follows:

$$T_{scale} = \frac{(T - T_{min})(T - T_{max})}{(T - T_{min})(T - T_{max}) - (T - T_{opt})^2} \quad (4)$$

where T_{opt}, T_{max}, T_{min} represent optimal, maximum, and minimum temperatures for photosynthesis activity for each vegetation class. Photosynthesis is assumed to be absent above or below T_{max} and

https://doi.org/10.5194/egusphere-2023-817
Preprint. Discussion started: 4 May 2023

T_{min}, respectively. T_{air} is the hourly air temperature at 2 m prescribed from ERA5 (Dee et al., 2011). In this study, we set T_{opt}, T_{min} and T_{max} to 20 °C, 0 °C and 45 °C, respectively. We utilise P_{scale} to account for the effects of leaf age on photosynthesis; hence it is set to 0 for water bodies and unclassified vegetation classes. P_{scale} is assumed to always be 1 for the Evergreen vegetation class. For all vegetation classes other than Evergreen, we compute P_{scale} as a function of LSWI except at the time of maximum greenness (representing full leaf expansion) as follows:

$$P_{scale} = \frac{1+LSWI}{2} \tag{5}$$

For the maximum greenness time, P_{scale} is set to 1.

W_{scale} is used to represent the effect of water stress on photosynthesis and is derived as follows:

$$W_{scale} = \frac{1+LSWI}{1+LSWI_{max}} \tag{6}$$

PAR is the photosynthetically Active Radiation, which is calculated based on incoming shortwave solar radiation (SW_{down}; µmol m^{-2} s^{-1}). SW_{down} is prescribed from ERA5.

In Eq. (3), T_{air} is constrained with a threshold value (T_{tshld}), and T_{air} below T_{tshld} is set to T_{tshld} for accounting for ecosystem respiration in winter times. Negative values of R_{eco} are set to 0.

The VPRM parameters, λ, SW_{down0}, α, and β are usually calibrated against site-level eddy covariance measurements across different ecosystem types by minimising the least squares between VPRM fluxes and eddy flux tower observations. This optimization procedure with discrete tower locations representing major vegetation classes is expected to enhance the model performance for the region of interest (Dayalu et al., 2018; Luus & Lin, 2015). Due to the lack of availability of sufficient observational eddy flux measurements for calibration for India, we use the VPRM parameters that were originally optimised against the Amazonian Tropical biomes (Botía et al., 2022) but modified as given in Table 2. We acknowledge that these parameters are not

https://doi.org/10.5194/egusphere-2023-817
Preprint. Discussion started: 4 May 2023

necessarily representing subtropical Indian biomes, which may lead to reduced model performance compared to other VPRM model simulations for regions like Europe or North America.

2.2 Ecosystem uptake refinements using SIF

As the reliability of the standard VPRM simulations depends on the model parameters, which are currently not specific to Indian biomes, we use satellite products based on OCO-2 and TROPOMI deriving the relationships between SIF and GPP across different vegetation classes and utilise them to improve the VPRM estimates of GPP.

We use two SIF products: GOSIF_v2 (http://data.globalecology.unh.edu/; Li & Xiao (2019a)), and the TROPOMI based product TROPOSIF (http://ftp.sron.nl/open-access-data-2/TROPOMI/tropomi/sif/v2.1/l2b/; Köhler et al. (2018)). GOSIF_v2 (hereafter referred to as GOSIF) provides SIF retrievals at spatial and temporal resolutions of 0.05° and 8-day. The spatial discontinuity in the original daily OCO-2 retrievals is improved in GOSIF using a machine learning approach based on MERRA-2 meteorological fields, MODIS reflectance and landcover data, preserving the observed variability of discrete SIF retrievals, as explained in (Li & Xiao, 2019a). In addition to SIF products, we also use the GPP product derived from OCO-2 SIF (Li & Xiao, 2019b), namely GOSIF_GPP_v2, providing 8-day GPP at 0.05° grid resolution for model comparison (see details below). Hourly SIF retrievals are available from TROPOMI (hereafter referred to as TROPOSIF) at 0.1° spatial resolution from May 2018 onwards.

We assumed GPP_{SIF} (i.e., GPP derived from SIF) to be varied linearly with SIF (Sun et al., 2017; Zhang et al., 2016). The SIF-GPP relationship across the vegetation classes in VPRM is derived as follows:

$$GPP_{SIF}(vg) = \gamma_{vg} \times SIF_{vg} + C_{vg} \quad (7)$$

https://doi.org/10.5194/egusphere-2023-817
Preprint. Discussion started: 4 May 2023

Here γ_{vg} is the factor converting SIF to GPP and C_{vg} represents the constant, specific to each biome vg. The biome specific γ_{vg} and C_{vg} over India are derived from the 8 day averaged OCO-2 derived GPP (GOSIF_GPP_v2) and SIF (GOSIF) products that followed the optimization procedure as described in Li & Xiao, (2019b), which are separated for each vegetation classes, denoted as $GPP_{OCO2}(vg)$ and $SIF_{OCO2}(vg)$. γ_{vg} and C_{vg} are thus the linear slope between $GPP_{OCO2}(vg)$ and $SIF_{OCO2}(vg)$, and the y-intercept respectively. When using TROPOSIF, the factor of difference between GOSIF and TROPOSIF values ($S_{GOSIF}(vg)$) is taken in to account to derive SIF-GPP relationship: i.e., $\gamma_{TROPOSIF,vg} = \gamma_{vg}/S_{GOSIF}(vg)$ and $C_{TROPOSIF,vg} = C_{vg}/S_{GOSIF}(vg)$ (see Sect. 3.1 for more details).

The distribution of GPP derived by the VPRM ($GPP_{vprm,STD}$) is improved by up-scaling it as follows:

$$GPP_{vprm,mod}(i,j,t,vg) = \eta_{vg} \times GPP_{vprm,STD}(i,j,t,vg) + \mathcal{E} \quad (8)$$

i, j, and t correspond to latitude, longitude, and time respectively. η_{vg} is the scaling factor corresponding to the specific vegetation class, applied to upscale $GPP_{vprm,STD}$ to include the information provided by SIF. η_{vg} is thus:

$$\eta_{vg} = \frac{\Sigma(GPP_{SIF}(vg) \times GPP_{vprm,STD}(vg))}{\Sigma GPP_{vprm,STD(vg)}{}^{2}} \quad (9)$$

2.3 Soil moisture and temperature in respiration model equation

The soil properties can influence both autotrophic and heterotrophic respiration, especially over a region with distinct wet and dry seasons (Flexas et al., 2006; Meir et al., 2008; Molchanov, 2009). Since the standard VPRM constructs ecosystem respiration as a simple linear function of air temperature, here we assess the impact of soil temperature and soil moisture (SM/ST) content in ecosystem respiration and refine the formulation accordingly. We utilise the SM/ST fields from

https://doi.org/10.5194/egusphere-2023-817
Preprint. Discussion started: 4 May 2023

the high-resolution land data assimilation system (HRLDAS; Chen et al. (2007)) based on the Noah land surface model (LSM), providing 3 hourly fields at 4 km spatial resolution for the period 2012 to 2017. As this data product does not cover our analysis period, we also use the SM fields from GLEAM v3 (https://www.gleam.eu/#datasets; Martens et al. (2017)) model and ST from ERA5 (https://cds.climate.copernicus.eu/cdsapp#!/dataset/reanalysis-era5-land?tab=overview; Hersbach et al. (2020)) reanalysis product (see Table 1).

The distribution of R_{eco} derived by the standard VPRM is re-defined as follows:

$$R_{eco,vprm,mod}(i,j,vg) = T_{s,vg}.ST(i,j,vg) + M_{s,vg}.SM(i,j,vg) + R_{vg}.\left(\alpha_{vg}.T_{air}(i,j,vg) + \beta_{vg}\right) \quad (10)$$

where, $T_{s,vg}$, $M_{s,vg}$ and R_{vg} represent the vegetation specific parameters derived using the multi-linear regression with soil temperature (ST), soil moisture (SM), and standard VPRM respiration against observation-based respiration fluxes. Here, we used two available observation-based datasets to calibrate respiration model parameters. The terrestrial vegetation fluxes (specifically ecosystem respiration fluxes) derived from 1) FLUXNET (https://db.cger.nies.go.jp/DL/10.17595/20200227.001.html.en, see Table 1, Zeng, Jiye (2020)) and 2) FLUXCOM (https://www.bgc-jena.mpg.de/geodb/projects/DataDnld.php, see Table 1, Jung et al. (2020)) observational database are used for parameter optimization. Table 2 provide the details of the vegetation specific model parameters derived for refining R_{eco}.

2.4 Other model products for comparison

For the inter-model comparison and performance assessment, we use simulated surface CO_2 fluxes from process-based terrestrial biosphere models commonly used for carbon cycle studies and the global inverse modelling system providing flux estimates consistent with atmospheric mixing ratio observations.

https://doi.org/10.5194/egusphere-2023-817
Preprint. Discussion started: 4 May 2023

We have used process-based simulations generated by 14 Dynamic Global Vegetation Models (DGVM's) employed in the TRENDYv10 model ensemble for the Indian region (see Table 3). All land surface models under TRENDY were driven with common input/forcing data from 1901 to 2020 and followed a common simulation protocol. Model simulations include climate forcing from CRU+CRU-JRA (https://crudata.uea.ac.uk/cru/data/hrg/cru_ts_4.05/) monthly and 6 hourly historical forcing for the period 1901 to 2020, ice core data from 1700 to 2020 and land-use change data from Hyde database for the period 850 to 2021. Specifically, this study uses TRENDY S3 simulation products, which consider the impact of atmospheric CO_2 concentration changes, climate change, and land cover changes on the global terrestrial ecosystem GPP (see https://blogs.exeter.ac.uk/trendy/). The TRENDY models used in this study differ in spatial resolution, but each provides fluxes at a monthly temporal resolution.

We use inverse model estimates of fluxes provided by the Carbon Tracker (CT2019B, hereafter referred to as CT) modelling system (https://gml.noaa.gov/ccgg/carbontracker/download.php; Peters et al. (2007)). The prior fluxes for the biospheric module of CT were from a diagnostic CASA biogeochemical model based on the remote-sensed monthly fraction of Photosynthetically Active Radiation (fPAR). Three hourly gridded estimates of optimised biospheric CO_2 fluxes with a horizontal resolution of 1°×1° over the Indian domain for the years 2016 to March 2019, available at https://gml.noaa.gov/ccgg/carbontracker/ are used in this study.

All these gridded flux estimates used for comparing spatial patterns are aggregated or disaggregated to a common spatial and monthly temporal resolution for comparison (see Sect. 2.6).

2.5 EC flux tower observations for model evaluation

For the model evaluation, we use eddy covariance observations of terrestrial biosphere CO_2 fluxes from a flux tower located at Betul (21°51'46.84" N latitude and 77°25'33.67" E longitude,

https://doi.org/10.5194/egusphere-2023-817
Preprint. Discussion started: 4 May 2023

Madhya Pradesh; Jha et al. (2013)) in the Central Indian state of Madhya Pradesh. Betul tower (commissioned in November 2011) is 507 m above mean sea level inside the mixed Deciduous forest where a tropical climate prevails. Further descriptions of the site and details of the instrumentation from Betul can be found in (Jha et al., 2013; Rodda et al., 2021). Table 4 provides an overview of the characteristics of the flux tower site, and Fig. 1 shows the location map of the flux towers under this study.

The half-hourly data from Betul is aggregated into hourly, daily, monthly and annual time scales for this analysis. All the available data from 2012 to July 2019 is used in this study (more details can be seen in Rodda et al. (2021)). There exist data gaps for specific years. For the evaluation analyses, model simulations are compared to observations at hourly, daily and monthly timescales. We estimate mean biases error (MBE), root mean squared error (RMSE), and squared correlation coefficient (R^2) to assess the model's efficiency in predicting the magnitude and variability.

2.6 Spatial and Biome-specific Pattern analysis

Here, we use flux simulations generated by refined VPRM, TRENDY model ensemble and CT, re-gridded to a spatial resolution of 1°×1°, to examine spatial gradients and seasonal variations of biospheric fluxes. Since some ecosystems can be more biologically productive than others, we aggregated flux patterns separately for each vegetation class based on SYNMAP land cover types for estimating each ecosystem's productivity in capturing atmospheric CO_2. We have also considered different periods, such as pre-monsoon (March to May), monsoon (June to September) and post-monsoon (October to December), to assess the seasonally varying biome productivity. We use improved VPRM fluxes at hourly time scales for these ecosystem-based analyses.

3. Results and Discussion

https://doi.org/10.5194/egusphere-2023-817
Preprint. Discussion started: 4 May 2023

3.1 Spatial and temporal patterns of SIF over Indian biomes

As explained in Sect. 2.2, we utilise satellite retrievals of SIF from OCO-2 (GOSIF) and TROPOMI (TROPOSIF) to improve VPRM-derived GPP ($GPP_{vprm,STD}$). Here, we present biome-specific analyses of SIF products, deducing their spatial and temporal characteristics over Indian biomes from 2018 to 2020. For the spatial analysis, the monthly and annual mean GOSIF data have been regirdded to 0.1°×0.1°. Both 8-day averaged SIF products agree with each other across biomes with R^2 ranging from 0.45 to 0.62 except for Grassland (R^2= 0.22) (see Table S1). A similar good agreement between SIF retrievals from OCO-2 and TROPOMI on global scale is also reported by Köhler et al. (2018) and Guanter et al. (2021).

Annually, the highest SIF values (GOSIF, mean/min/max: 0.28/0.03/0.44 mW m^{-2} sr^{-1} nm^{-1} and TROPOSIF, mean/min./max: 1.18/0.17/1.93 mW m^{-2} sr^{-1} nm^{-1} for the year 2019) are exhibited by Evergreen forest, and the lowest values are observed (GOSIF, mean/min/max: 0.07/0/0.24 mW m^{-2} sr^{-1} nm^{-1}, TROPOSIF, mean/min/max: 0.41/0/1.61 mW m^{-2} sr^{-1} nm^{-1}) over the desert regions of Rajasthan where Shrubland vegetation dominates. Over the years (2019 to 2020), based on GOSIF, the rates of an annual increase in SIF value for Cropland, Savanna, Shrubland, Deciduous forest, and Evergreen forest are in the range of 0.01 mW m^{-2} sr^{-1} nm^{-1} to 0.23 mW m^{-2} sr^{-1} nm^{-1}, with Grassland showing no enhancement. Mixed Forest biomes exhibit a negative growth rate of -0.005 mW m^{-2} sr^{-1} nm^{-1}. Like GOSIF, TROPOSIF also indicates zero growth rate for Grasslands, while other ecosystems show an annual growth rate between 0.04 mW m^{-2} sr^{-1} nm^{-1} to 0.11 mW m^{-2} sr^{-1} nm^{-1}. On an annual scale, large spatial variability in the SIF values is exhibited by Shrubland and the least by Savanna. Overall, we find that TROPOSIF values (based on SIF retrievals at 735 nm) are ~4 times greater than GOSIF (based on SIF retrievals at 757 nm) over the study region for all the biomes except for Grassland, where the biome-specific TROPOSIF is ~3

https://doi.org/10.5194/egusphere-2023-817
Preprint. Discussion started: 4 May 2023

times larger than GOSIF. Hence, we scaled up GOSIF and the derived scaling factors are specific to each biome (see Table S1). A similar up scaling of OCO-2 SIF is also done by Köhler et al. (2018) and Guanter et al. (2021) for comparing the fields with TROPOSIF on a global scale. In Fig. 2, we compare scaled GOSIF and TROPOSIF across different biomes.

We find that the spatial heterogeneity observed in SIF emission is directly related to the vegetation class and the availability of rainfall. For example, biomes in Central, North East and South West India, where significant rainfall occurs during the summer monsoon period (June - August), show higher fluorescence than the rest of the region (see Fig. 3). All vegetation classes exhibit large seasonal variability with a seasonal maximum from June to July and a seasonal minimum from March to April (see Fig. 4), indicating changes in the rate of photosynthesis with rainfall availability with correlation values ranging from 0.78 to 0.93. A similar high positive correlation between precipitation and SIF is indicated by Albright et al. (2022) over the Amazon region. No significant influence of rainfall is found in the seasonality over Grassland (R^2 = <0.4). Cropland and Shrubland vegetation show the primary maximum with the onset of monsoon (June-July) and the secondary maximum during winter months (January-February). These two seasonal maxima are consistent with the prominent crop-growing seasons of India (Nayak et al., 2010), which are associated with enhanced primary productivity. Compared to GOSIF, TROPOSIF better exhibits the double peak in SIF temporal distribution for both ecosystems over this region.

3.2 SIF-GPP relationship across different biomes

We have derived SIF-GPP relationship similar to Li & Xiao (2019b) using up scaled GOSIF and GPP_{SIF} across different biomes over India, as mentioned in Sect. 2.2 (see Table 5). Li & Xiao (2019b) used linear relationship between GOSIF flux tower network of observations (FLUXNET; Baldocchi et al. (2001)) based GPP to map GPP globally. Our derived scalars for converting SIF to GPP are different from Li & Xiao (2019b) due to the differences in Indian biomes, their

https://doi.org/10.5194/egusphere-2023-817
Preprint. Discussion started: 4 May 2023

classifications, and the up-scaling of the GOSIF product (see Table 5). The derived scalars for converting SIF to GPP range from 4.80 to 7.84 mW m^{-2} sr^{-1} nm^{-1}/µmol m^{-2} s^{-1} for different biomes. While both SIF patterns are in good agreement with VPRM-derived GPP over most of the vegetation classes under our study (e.g., R^2 = 0.77 to 0.85 for Shrubland), we find a weak correlation between SIFs and standard VPRM-derived GPP for Savanna (R^2 = 0.09 to 0.36). The above correlation values are based on the annually averaged data analysis from 2018 to 2019 (not shown).

3.3 Model evaluation with eddy covariance flux observations

Figure 5 shows the inter-annual variations in monthly averaged fluxes of GPP, R_{eco}, and NEE over Betul from 2012 to 2018. A significant data gap exists during 2014 and 2017. Since Betul is a tropical Deciduous forest, the strong seasonality exhibited by the observed fluxes can be associated with changes in plant physiology throughout the year. Based on Betul observations, Rodda et al. (2021) reports a net sink at site level with an annual NEE, GPP and R_{eco} of -524 ± 40 g C m^{-2} yr^{-1}, 3358 ± 167 g C m^{-2} yr^{-1}, and 2834 ± 157 g C m^{-2} yr^{-1}, respectively. While observed NEE shows positive values (representing carbon release to the atmosphere) during summer (March - June), the ecosystem uptake was observed (negative NEE values) for the rest of the year (July - February). Seasonal maxima for GPP range from 19 µmol m^{-2} s^{-1} to 25 µmol m^{-2} s^{-1} from July to September due to peak photosynthetic activity associated with optimal water and moisture availability. The forest site receives rain from June onwards, with maximum precipitation during July (South West monsoon period, based on TRMM precipitation data). However, the ecosystem productivity is less in June due to a shortage in photosynthetically active solar radiation owing to cloud cover, as seen from satellite images (https://www.mosdac.gov.in/). Also, the transition in vegetation development from dry summer to wet periods occurs during the early monsoon month (June). The availability of rainfall and radiation enhances plant productivity at the site, Rodda et

https://doi.org/10.5194/egusphere-2023-817
Preprint. Discussion started: 4 May 2023

al. (2021) noted. The variability in seasonal maxima over the year can thus be associated with the inter-annual variability of the summer monsoon. Ecosystem productivity reaches its annual minimum during March and April (1 µmol m^{-2} s^{-1} to 3 µmol m^{-2} s^{-1}) due to the leaf shedding of Deciduous vegetation during summer. Ecosystem respiration showed two peaks, a primary peak during early monsoon months (June & July) and a secondary peak during late monsoon months (August & September). These respiration peaks are associated with increased air temperature when autotrophic respiration is expected to increase and enhanced soil microbial respiration when attaining sufficient soil moisture. An increase in vegetation greenness with water availability also enhances autotrophic respiration. A sharp fall in R_{eco} after the primary maxima can likely be due to the decrease in soil respiration due to water logging associated with enhanced precipitation creating anoxic conditions and limiting microbial activity in the area (Han et al., 2018). The conditions become favourable for autotrophic and heterotrophic respiration during post-monsoon (enhanced vegetation greenness and optimal soil moisture content), resulting in the observed secondary maximum. We find weak ecosystem respiration from November to May (2 µmol m^{-2} s^{-1} to 7 µmol m^{-2} s^{-1}) owing to the leaves shedding and reduced soil respiration, limited by dry soil.

On comparing observations with model simulations, standard VPRM (hereafter referred to as $VPRM_{STD}$) shows better agreement in predicting the seasonality in observed monthly averaged NEE fluxes (R^2 = 0.59) than CT (R^2 = 0.24) and TRENDY (R^2 = 0.45), but with a significant underestimation of NEE fluxes at a monthly scale (see Table 6). The model bias increases from August to December (MBE = 4.83 µmol m^{-2} s^{-1} and RMSE = 5.0 µmol m^{-2} s^{-1}) compared to other periods. Note that we have used the TRENDY model ensemble for the comparison, and the variation among TRENDY model simulations for NEE (as calculated by the standard deviation from the ensemble mean over the seven years) ranges from -2.84 µmol m^{-2} s^{-1} to 1.80 µmol m^{-2} s^{-1} over Betul. Similar to NEE, the model predicted the monthly mean variations in GPP reasonably

https://doi.org/10.5194/egusphere-2023-817
Preprint. Discussion started: 4 May 2023

well (R^2 = 0.71), but with considerable bias (MBE = -6.7 µmol m^{-2} s^{-1}, RMSE = 8.3 µmol m^{-2} s^{-1}). The model-observation bias for GPP is found to be high during productive months (June-December). Previous studies have shown the underestimation of GPP when MODIS-derived products are used for GPP estimation (e.g., Zhang et al., 2008). The GPP underestimation by $VPRM_{STD}$ can be thus related to the usage of MODIS reflectance products. Overall, $VPRM_{STD}$ captures the seasonal pattern in NEE and GPP compared to other biospheric models with different model structures, such as the inversion product CT and the ensemble of process-based models TRENDY.

We further investigated reducing the model-observation bias in the $VPRM_{STD}$ model. In addition to standard datasets in $VPRM_{STD}$, we utilised GPP_{SIF} products, soil moisture and soil temperature to improve GPP and R_{eco} simulations. Incorporating SIF in simulating the VPRM GPP has noticeably improved the ability of the model to capture the observed seasonal variability (see Fig. 5). Both GPP_{GOSIF} and $GPP_{TROPOSIF}$ show good agreement in capturing the seasonal variations (R^2 = 0.65 to 0.68), with values closer to the observation. Though SIF based GPP products are closer than $GPP_{vprm,STD}$ to the observed GPP in terms of magnitude, the observed patterns in GPP are better captured by $VPRM_{STD}$ (R^2 >0.7) than other products (see Sect. 3.3). This shows the potential of VPRM model to predict the observed variations in GPP, leading to calibrate VPRM model parameters rather simply using GPP_{GOSIF} and $GPP_{TROPOSIF}$ in our NEE estimations. VPRM GPP modified based on GOSIF (hereafter referred to as $VPRM_{GOSIF}$), and VPRM modified based on TROPOSIF (hereafter referred to as $VPRM_{TROPOSIF}$) are evaluated with observations, and the inter-comparison with $VPRM_{STD}$ shows remarkable improvement in the model performance for GPP with a significant reduction in RMSE and MBE values (see Fig. 5a and Table 6). For GPP, the bias reduced significantly for refined models (RMSE: $VPRM_{GOSIF}$ = 4.9 µmol m^{-2} s^{-1}, and

https://doi.org/10.5194/egusphere-2023-817
Preprint. Discussion started: 4 May 2023

$VPRM_{TROPOSIF}$ = 4.3 µmol m^{-2} s^{-1} and MBE: $VPRM_{GOSIF}$ = -3.3 µmol m^{-2} s^{-1}, $VPRM_{TROPOSIF}$ = -2.6 µmol m^{-2} s^{-1}). The observed seasonal anomalies in GPP (variability after subtracting the decadal mean), associated with ecosystem stress and phenology, ranges from -7.0 to 17.0 µmol m^{-2} s^{-1} with a standard deviation of 6.3 µmol m^{-2} s^{-1}. These variations are well captured by our model with a mean bias of -1.8 µmol m^{-2} s^{-1}. The above levels of model improvements confirm the potential of using high-resolution satellite-derived SIF in capturing the seasonal cycle of GPP at an ecosystem level. Hence, our results are broadly consistent with Qiu et al. (2020); Joiner et al. (2018); and Wood et al. (2017). As a direct proxy for photosynthesis, SIF is expected to provide improved estimates than conventional vegetation indices (Zhang et al., 2016) (e.g., EVI, LSWI) used in VPRM GPP estimation.

The $VPRM_{STD}$ model fails to capture the seasonality in respiratory fluxes (R^2 = 0.02) for the period from 2012 to 2018, with a significant underestimation of ecosystem respiration by -3.5 µmol m^{-2} s^{-1} (RMSE values: ~5.7 µmol m^{-2} s^{-1}). To improve the model performance, we performed three sets of modified VPRM simulations for R_{eco}, utilising observation-based datasets in addition to those already used for $VPRM_{STD}$ R_{eco} simulations, such as 1. ST, 2. SM, and 3. both ST and SM. R_{eco} modified based on various datasets (e.g., HRLDAS ST/SM, ERA5 ST, and GLEAM SM) provide similar results. Here we present the analysis using ERA5 ST and GLEAM SM, considering the large temporal coverage of the data. VPRM respiration modified using SM (Fig. 5b) shows much improvement in model prediction (R^2: 0.80) than when ST alone is used. VPRM respiration modified using both SM and ST (i.e., $VPRM_{MOD}$) shows slightly better improvement than using only SM. The model-observation bias reduced considerably, with RMSE reducing from 5.7 µmol m^{-2} s^{-1} to 1.9 µmol m^{-2} s^{-1} and MBE reducing from -3.5 µmol m^{-2} s^{-1} to -0.01 µmol m^{-2} s^{-1}. In general, incorporating the soil temperature and soil moisture in addition to air temperature in the ecosystem respiration calculation in the VPRM improves the model's ability to simulate more realistic values

https://doi.org/10.5194/egusphere-2023-817
Preprint. Discussion started: 4 May 2023

over the Deciduous ecosystem of Betul. The improvement in VPRM R_{eco} while incorporating soil temperature is also reported elsewhere (e.g., Luus et al., 2015).

The VPRM NEE estimated based on modified GPP from $VPRM_{GOSIF}$ and R_{eco} from $VPRM_{MOD}$ (hereafter referred to as $VPRM_{GOSIF,SMST}$) and based on $VPRM_{TROPOSIF}$ and $VPRM_{MOD}$ (hereafter referred to as $VPRM_{TROPOSIF,SMST}$) are evaluated with observation over Betul (Fig. 5c). The modified models showed improvement over $VPRM_{STD}$ in capturing the observed seasonal pattern with a reduction in errors during the period from 2012 to 2018 (RMSE: $VPRM_{GOSIF,SMST}$ = 4.4 µmol m^{-2} s^{-1}, $VPRM_{TROPOSIF,SMST}$ = 3.8 µmol m^{-2} $s^{-1}$and MBE: $VPRM_{GOSIF,SMST}$ = 3.2 µmol m^{-2} s^{-1}, $VPRM_{TROPOSIF,SMST}$ = 2.4 µmol m^{-2} s^{-1}) (see Table 6). The observed seasonal anomalies in NEE ranges from -4.9 to 8. µmol m^{-2} s^{-1} with a standard deviation of 3.6 µmol m^{-2} s^{-1}. These variations are well captured by our model with a mean bias of 1.6 µmol m^{-2} s^{-1}. The modifications made to VPRM GPP and R_{eco} fluxes improved the model's ability to capture NEE fluxes over Betul.

Since $VPRM_{TROPOSIF,SMST}$ is found to be closer to the observation among other modified VPRM models, the rest of the analysis uses the simulations from $VPRM_{TROPOSIF,SMST}$ (hereafter referred to as $VPRM_{refined}$).

3.4 Flux spatial patterns

We find strong spatial variations in the NEE and GPP estimates by $VPRM_{refined}$ over the Indian region (see Figs. 6 and 7), with distinct zonal and meridional variations. These variations are expected, resulting from factors such as patterns in annual mean temperature, precipitation, and radiation which can have significant influences on the spatial pattern of ecosystem carbon fluxes (e.g., Yu et al., 2013). The inter-annual variability in simulated NEE during the study period is highly correlated (R^2>0.5) with the interannual variability in the country's precipitation pattern, which is in line with Dadhwal, 2012. Annually, most of the country's biomes remained as a net carbon sink, with higher NEE values over the southwest and northeast regions, which are

https://doi.org/10.5194/egusphere-2023-817
Preprint. Discussion started: 4 May 2023

dominated by Evergreen and Mixed forest ecosystems. The highest GPP values are also found in these regions, marking the highest productive biomes. Comparatively, high GPP is observed in the eastern part of central India, where the Deciduous ecosystem prevails. However, respiration exceeds primary productivity over the above region, leaving it as a carbon source on an annual scale. A major part of the country shows moderate GPP values (~0.08 kg C m^{-2} $month^{-1}$ to 0.15 kg C m^{-2} $month^{-1}$), while a large area is covered by cropland vegetation. Ecosystem productivity is minimal in the northern and north western parts of the country under Shrubland vegetation.

During the period from 2012 to 2020, the Indian terrestrial biosphere acted as a net carbon sink annually. The NEE value ranges from -0.38 Pg C yr^{-1} to -0.51 Pg C yr^{-1} in 2012 to -0.53 Pg C yr^{-1} to -0.64 Pg C yr^{-1} in 2020 (see Fig. 6). The inter-comparison of total NEE fluxes are lower in CT and TRENDY compared to those of $VPRM_{refined}$ ($\mu_{(VPRM_{refined}-\mathrm{CT})}$ = -0.34 Pg C yr^{-1}; $\mu_{(VPRM_{refined}-\mathrm{CT})}$ = -0.25 Pg C yr^{-1} in which μ represents sample mean of differences). The NEE differences reported above used $VPRM_{refined}$ respiration model parameters calibrated using FLUXNET. The corresponding NEE differences when using FLUXCOM are: $\mu_{(VPRM_{refined}-\mathrm{CT})}$ = -0.52 Pg C yr^{-1}; $\mu_{(VPRM_{refined}-\mathrm{CT})}$ = -0.41 Pg C yr^{-1}. An ensemble means using 14 TRENDY models is used for the analysis and the above reported values are based on the year 2018. Our NEE estimates (see Fig. 6) are higher than the previously published studies in which process-based and light-use efficiency models were used (Cervarich et al., 2016; Nayak et al., 2015; Rao et al., 2019). Based on the CASA model, Nayak et al. (2015) estimated a NEE value of -0.0098 Pg C yr^{-1} for a 26-year period from 1981 to 2006, showing ecosystem transition from a carbon source in the 1980s to a carbon sink in the subsequent decades. Using a process-based model ensemble, namely TRENDY, Cervarich et al. (2016) estimated an annual NEE value of -0.2 Pg C yr^{-1} from 2000 to

https://doi.org/10.5194/egusphere-2023-817
Preprint. Discussion started: 4 May 2023

2013. A similar study using TRENDY models by Rao et al. (2019) also showed the uptake capacity of the Indian region by -0.14 Pg C yr^{-1} from 1901 to 2010.

The spatial patterns for monthly averaged NEE and GPP are presented in Fig. 7. The highest values for NEE and GPP are found during the months of July to September i.e., the summer monsoon season and the lowest values are found during the dry and hot months from March to May (Fig. 7). The Indo-Gangetic plain shows higher NEE values during the winter months and summer monsoon seasons. This coincides with the highest productivity associated with the peak growing stage of the two major cropping seasons in India. Enhanced NEE and GPP values across the entire Indian region from June to September are associated with enhanced agricultural crop production based on the availability of monsoonal rainfall. The south eastern part of the country shows an increase in NEE and GPP values as a result of increased productivity upon the commencement of the North East winter monsoon. Most parts of the country remained carbon neutral from March to May. Winter crop harvesting and unfavourable conditions for plant growth (e.g., high temperature, low water availability, low soil moisture content etc.) resulted in minimum productivity during this period. A major part of Deciduous vegetation persisted as a source throughout the seasons. Even though Deciduous vegetation shows higher seasonality and GPP values, ecosystem respiration dominates GPP across this biome, leaving it as a carbon source or carbon neutral on an annual scale (e.g., Deb Burman et al., 2021; Sarma et al., 2022).

3.5 Derived ecosystem productivity and exchanges across different biomes

Here, we present the derived ecosystem productivity and exchange fluxes across seven vegetation classes used in VPRM (Table 7). Large variability in ecosystem productivity is found on different temporal scales. On an annual scale, the Mixed forest vegetation shows the highest

https://doi.org/10.5194/egusphere-2023-817
Preprint. Discussion started: 4 May 2023

(GPP = 6.35 kg C m^{-2} yr^{-1}) productivity, followed by the Evergreen forest, Deciduous forest and Savanna biomes (GPP = 5.51 kg C m^{-2} yr^{-1}, 4.63 kg C m^{-2} yr^{-1}, 4.60 kg C m^{-2} yr^{-1}, respectively). Figure 8 presents the spatial pattern in annually averaged GPP over different vegetation for the year 2020. The GPP distribution is found to be spatially heterogeneous and is influenced by local geographic and climatic factors. The spatial distribution of GPP also exhibits inter-annual variations (see Fig. S2). As expected, lower productivity rates are found for Shrubland (1.74 kg C m^{-2} yr^{-1}) and Cropland (1.43 kg C m^{-2} yr^{-1}). Cropland covers more than 68% of Indian land mass. However, the total Cropland GPP is found to be lower than Deciduous forests (area coverage: 4.4%), Evergreen (area coverage: 4.8%) and Mixed forests (area coverage: 3.7%), while the total area covered by these vegetation classes is small. The lowest annual productivity is seen over the Grassland with a GPP value of 0.66 kg C m^{-2} yr^{-1}. Even though higher productivity is associated with Deciduous forest, this biome results in less net carbon uptake due to the high respiration fluxes of this vegetation. The highest productivity of forest ecosystems over Grassland is also seen in other parts of the globe (e.g., Yu et al., 2013). The contribution of each vegetation to the national GPP budget also depends on the area covered by each vegetation. As a result, to the national GPP budget of 3.88 Pg C yr^{-1}, for the year 2020, Cropland is the major contributor (49.6%), followed by Evergreen forest (14.9%), Mixed forest (12.2%), Shrubland (12.0%), Deciduous forest (9.3%), Savanna (1.1%) and Grassland (0.5%). Figure 9.a shows the annual mean GPP from different vegetation classes from 2012 to 2020. On an annual scale, Mixed and Evergreen forest vegetation groups show large GPP variability, while Cropland and Grassland exhibit lower GPP variability. This variability across biomes remains consistent over the years during the analysis period.

Evergreen Forest is the largest contributor to the national NEE budget (~39.7%) followed by Cropland (~33.6%), Mixed Forest (~31.5%), Shrubland (~10.7%), Savanna (~1.1%), Grassland

https://doi.org/10.5194/egusphere-2023-817
Preprint. Discussion started: 4 May 2023

(~-0.2%), and Deciduous forest (~-17.3%), based on the data from 2020. The Evergreen forest and Mixed forest vegetation are with the highest carbon fixation sink capacity, showing high NEE values (see Table 7) (NEE of ~-2.4 kg C m^{-2} yr^{-1}), followed by Savanna with an annual NEE value of ~-1.3 kg C m^{-2} yr^{-1}. A Moderate net carbon fixation efficiency (NEE of ~-0.3 and – 0.2 kg C m^{-2} yr^{-1}) is shown by Shrubland and Cropland vegetations, respectively. The above reported values are based on $VPRM_{refined}$ in which respiration and model parameters are calibrated using FLUXNET. The lowest efficiency is found for Deciduous vegetation, indicating a carbon-neutral biome. Evergreen and Mixed forest ecosystems persisted as net sinks throughout the seasons with higher productivity (Fig. 8). Figure 9.b shows the annual mean NEE from different vegetation classes from 2012 to 2020. On an annual scale, Mixed and Evergreen forest vegetation groups show large NEE variability while lowest by the Cropland and Grassland. Similar to GPP, the variability found across biomes remains consistent over the years during the analysis period with interannual variations. It is also seen that over the years sink capacity of most of the vegetation has increased.

3.6 Seasonal and diurnal cycles across different biomes

Figure 10 shows the seasonal variations in $VPRM_{refined}$ simulated NEE fluxes across different biomes from 2012 to 2020. The seasonality varies across the vegetation. Vegetations such as Cropland, Savanna, and Shrubland show similar seasonal carbon dynamics with higher NEE from September to October and lower NEE from April to May. These biomes remained as carbon sinks throughout the year except for March to May. On the other hand, Grassland shows higher NEE from July to August and lower NEE from November to January. Even though Mixed forests show seasonal variations, it is not consistent over the years. Throughout the year, Grassland, Cropland, Evergreen forest, and Mixed forest remained as a net carbon sink. On the other hand, Deciduous vegetation remained a carbon source as ecosystem respiration surpassed primary

https://doi.org/10.5194/egusphere-2023-817
Preprint. Discussion started: 4 May 2023

production. Strong seasonality in NEE is exhibited by Savanna (11.94 µmol m^{-2} s^{-1}), followed by Mixed forest (10.57 µmol m^{-2} s^{-1}), while the least is observed for Cropland (3.38 µmol m^{-2} s^{-1}) (Statistics presented for the year 2020). For each vegetation, the spatial heterogeneity in NEE values is more during those months showing higher uptake capacity (Fig. not shown).

We find that the seasonality in the ecosystem uptake is associated with the wet and dry conditions, showing a transition from dry and cooler winter months to wet and hot summer months (see Fig. S3). The majority of the vegetation shows higher productivity during August to September and lowest during March to May (e.g., Cropland, Savanna, Deciduous forest, Evergreen forest, Mixed forest, and Shrubland). The ecosystems show a semi-annual cycle with a primary productivity peak during the winter months (December - January) and a secondary peak during the monsoon season (August - September). Productivity of Grassland remained high from June onwards and lasted till August. For 2020, the Savanna shows strong seasonality with 18.6 µmol m^{-2} s^{-1} variation in GPP value from low to high productive month followed by Deciduous and Mixed forest groups (16.57 µmol m^{-2} s^{-1}, 12.01 µmol m^{-2} s^{-1}, respectively). Grassland shows the lowest variation in GPP with the season (3.83 µmol m^{-2} s^{-1}). Also, the magnitude of seasonal variability remains low for vegetations such as Cropland (5.05 µmol m^{-2} s^{-1}) and Savanna (5.29 µmol m^{-2} s^{-1}).

Figure 11 shows the diurnal variations in $VPRM_{refined}$ simulated GPP fluxes at a monthly scale for different vegetation classes during 2020. The diurnal variability of GPP varies with the season. A seasonal shift in the peak uptake time is found, and it varies with vegetation. Larger productivity is found during noon hours (10:00 -14:00 local time), of summer monsoon months of August and September and the post-monsoon months of October and November. The productivity gradually decreases with the progress of the dry season. The lowest GPP values are found during March and May. Strong daytime variability, with peak uptake during early morning hours and weak

https://doi.org/10.5194/egusphere-2023-817
Preprint. Discussion started: 4 May 2023

uptake during afternoon hours, is also found during this dry season, indicating the temperature dependence on ecosystem productivity, which also varies with biome type and age.

4. Conclusion:

This study presents the terrestrial flux distribution of CO_2 over India on a 0.1°×0.1° grid at a temporal resolution of 1 hour from 2012 to 2020. We utilise satellite-based vegetation and ecosystem productivity indices and high-resolution meteorological data in a data-driven biospheric model to improve the model estimates of terrestrial biosphere CO_2 flux components over India. In particular, we take advantage of satellite missions, such as TROPOMI and OCO-2 providing retrievals of solar-induced chlorophyll fluorescence (SIF) and relate them to ecosystem productivity across different biomes. The derived flux products better explain the magnitude and fine-scale variability over the region compared to other existing model estimates.

We investigated how our model captures the seasonal pattern in NEE and GPP compared to other biospheric models with different model structures, such as the inversion product CT and the ensemble of process-based models TRENDY. Though $VPRM_{STD}$ shows better agreement with observations in predicting the seasonality of NEE fluxes (R^2 = 0.59) than CT (R^2 = 0.24) and TRENDY (R^2 = 0.45) for the period from 2012 to 2018, the simulations considerably underestimated the NEE fluxes at a monthly scale, with model biases of 3.2 µmol m^{-2} s^{-1} for NEE and -6.7 µmol m^{-2} s^{-1} for GPP. The model-observation bias is high for simulating GPP during productive months (June - December). We infer that the GPP underestimation by $VPRM_{STD}$ can be related to the MODIS reflectance products and the plausible errors in model parameters. The $VPRM_{STD}$ model parameters are not optimised using flux tower measurements due to the unavailability of flux observations over the Indian sub-continent, thereby limiting the model performance over the domain while using uncalibrated model.

https://doi.org/10.5194/egusphere-2023-817
Preprint. Discussion started: 4 May 2023

We performed biome-specific analyses of SIF products, deducing their spatial and temporal characteristics over Indian biomes and applied them to $VPRM_{STD}$. Compared to other process-based biospheric models and atmospheric inversion products, the refined VPRM shows remarkable performance in explaining small-scale variability. By improving GPP and R_{eco} simulations, the model has improved its ability to capture the observed NEE fluxes (R^2>0.5) with a significant reduction in RMSE (~3 µmol m^{-2} s^{-1}) and MBE (~3 µmol m^{-2} s^{-1}) values. While evaluating $VPRM_{refined}$ GPP with observation-based GPP at the Betul site, we find better model performance compared to $VPRM_{STD}$ with reduced bias (RMSE = 4.3 µmol m^{-2} s^{-1} and MBE = -2.6 µmol m^{-2} s^{-1}). The monthly variations in GPP (R^2>0.7) and R_{eco} (R^2>0.8) are better captured by $VPRM_{refined}$ than other models. The $VPRM_{refined}$ reproduces the seasonal anomalies exhibited by Betul observations remarkably well, for example, with explained variability of GPP and NEE anomalies by 85% and 68%, respectively from 2014 to 2018. However, the model evaluation is limited only to the Deciduous ecosystem due to the observational constraints that are only representative of the above ecosystem.

We find significant spatial variations in the NEE and GPP flux distributions simulated by $VPRM_{refined}$, which are associated with the spatial heterogeneity in annual mean temperature, precipitation, and radiation. Evergreen and Mixed forests covering southwest and northeast of India show the highest productivity annually. Ecosystem productivity is minimal in the northern and north western parts of the country (mainly Shrubland vegetation). The Deciduous forest remained as an annual carbon source despite the high productivity due to higher respiratory fluxes. NEE and GPP fluxes show higher values during July to September (i.e., the summer monsoon season) and lower values during March to May (dry and hot months), and these seasonal variations are in line with the seasonal variations in the rain, temperature, and solar radiation. Since more than 60% of the country is covered with Croplands, the agricultural pattern also influences the seasonality in

https://doi.org/10.5194/egusphere-2023-817
Preprint. Discussion started: 4 May 2023

GPP and NEE. Overall, we find that the Indian biosphere acts as a sink with an annual NEE ranging from -0.38 Pg C yr^{-1} (-0.51 Pg C yr^{-1}) to -0.53 Pg C yr^{-1} (-0.88 Pg C yr^{-1}) when the respiration model parameters calibrated using FLUXNET (FLUXCOM) and an annual GPP ranging 3.39 yr^{-1} to 3.88 Pg C yr^{-1} for the years from 2012 to 2020.

Though we have demonstrated the use of additional satellite-based observations and provided the high-resolution gridded CO_2 flux distributions, future work evaluating the simulated flux distribution with an adequate number of flux site observations and atmospheric CO_2 mixing ratio is warranted. Potential improvements to VPRM include i) further refinement in the ecosystem respiration accounting for moisture and heat stress and other biomass disturbance and ii) incorporating flux observations from different ecosystems to enhance the flux representativeness with better empirically derived and biome-specific model parameters. The increased number of flux tower observations in the future will help to optimise the model parameters to enhance the robustness of these simulations.

Given the considerable difference in flux components among the terrestrial biospheric models, the analyses demonstrated here can guide future model improvements in deriving GPP and ecosystem respiration. By showing the potential of VPRM model to predict the observed variations in GPP better than solely SIF-based GPP products, the present study demonstrates the way to calibrate the VPRM model parameters in the absence of eddy covariance measurements. The next step would be to combine atmospheric data and VPRM through inverse modelling to better understand the Indian carbon balance.

https://doi.org/10.5194/egusphere-2023-817
Preprint. Discussion started: 4 May 2023

Data availability

The VPRM simulations will be made available upon request to the corresponding author. The Carbon Tracker (CT2019B) is freely available online at https://gml.noaa.gov/ccgg/carbontracker/CT2019B/. TRENDYv10 datasets used in this study are available upon request to S. Sitch. Eddy covariance observation data may be available upon request to NRSC; https://www.nrsc.gov.in/. The TROPOMI data is available online at http://ftp.sron.nl/open-access-data-2/TROPOMI/tropomi/sif/v2.1/l2b/. GOSIF_v2 datasets used are available freely from http://data.globalecology.unh.edu/. ERA5 data used is freely available at https://cds.climate.copernicus.eu/cdsapp#!/dataset/reanalysis-era5-land?tab=overview. GLEAM v3 data is available freely at https://www.gleam.eu/#datasets. FLUXNET data is available freely from https://db.cger.nies.go.jp/DL/10.17595/20200227.001.html.en. FLUXCCOM data used is freely available from https://www.bgc-jena.mpg.de/geodb/projects/DataDnld.php. TRMM precipitation data used is available freely from https://disc.gsfc.nasa.gov/datasets/TRMM_3B42_Daily_7/summary.

Authors contribution

Aparnna Ravi: Method development, Coding, Data processing, Analysis, Visualization, Writing – original draft preparation, Dhanyalekshmi Pillai: Conceptualization, Method development, and Writing - review & editing, Christoph Gerbig: Data processing and Writing - review & editing, Vishnu Thilakan: Analysis and Writing - review & editing, Stephan Sitch: Model data and Writing - review & editing, Sönke Zaehle: Writing - review & editing, Chandrashekhar Jha: EC flux tower data acquisition and processing and Writing - review & editing

Declaration of Competing Interest

The authors affirm that they have no known financial or interpersonal conflicts that would have appeared to have an impact on the research presented in this study.

https://doi.org/10.5194/egusphere-2023-817
Preprint. Discussion started: 4 May 2023

Acknowledgements

This study has been funded by the Max Planck Society allocated to the Max Planck Partner Group at IISERB. DP acknowledges the support from the Science and Engineering Research Board (SERB) through an Early Career Research Award (grant no. ECR/2018/001111) for generating some data products used in the study. AR acknowledges the support of IISERB's high-performance cluster system for computations, data analysis, and visualization. AR and VT are grateful to the Ministry of Human Resource Development (MHRD, India) for their PhD scholarships. We thank National Remote Sensing Centre (NRSC), Hyderabad, for providing access to Betul EC flux tower data, and we acknowledge the efforts of scientists and technicians from the Forestry and Ecology Group at NRSC Hyderabad for the EC data acquisition.

https://doi.org/10.5194/egusphere-2023-817
Preprint. Discussion started: 4 May 2023

Tables

Table 1: An overview of the observational- and model- based datasets used in this study.

Dataset	Products	Spatial resolution	Temporal resolution	Period	Reference
VPRM	GPP, NEE, R_{eco}	0.1°×0.1°	Hourly	2012 - 2020	(Mahadevan et al., 2008)
TROPOMI	SIF	0.1°×0.1°	Hourly	2018 - 2020	(Köhler et al., 2018)
GOSIF_v2	SIF	0.05°×0.05°	8 day	2016-2020	(Li & Xiao, 2019a)
ERA5	ST	0.1°×0.1°	Hourly	2012-2020	(Hersbach et al., 2020)
GLEAM v3	SM	0.25°×0.25°	Daily	2012-2020	(Martens et al., 2017)
HRLDAS	ST and SM	$0.03^0\times0.03^0$	3 hourly	2012- 2017	(Chen et al., 2007)
Gridded R_{eco} from FLUXNET	R_{eco}	$0.1^0\times0.1^0$	10 days	2012-2019	(Zeng, Jiye, 2020)
FLUXCOM	R_{eco}	$0.5^0\times0.5^0$	Monthly	2012-2019	(Jung et al.,

https://doi.org/10.5194/egusphere-2023-817
Preprint. Discussion started: 4 May 2023

					2020)
EC	NEE, GPP, R_{eco}	1 km^2	Half hourly	2012-July 2019	(Jha et al., 2013)
CT2019B	NEE	1°×1°	Three hourly	2012 – March 2019	(Peters et al., 2007)
TRENDYv10	NEE, GPP, R_{eco}	Vary with model	Monthly	2012 - 2020	Ref. Table 2
GOSIF_GPP_v2	GPP	0.05°×0.05°	8 day	2016-2020	(Li & Xiao, 2019b)
TRMM	Rainfall	0.25°×0.25°	Daily	2016 - 2019	(Kummerow et al., 2000)

https://doi.org/10.5194/egusphere-2023-817
Preprint. Discussion started: 4 May 2023

Table 2. List of VPRM (both standard and refined) parameters and vegetation classes used in this study. a. respiration model parameters calibrated FLUXNET; b. respiration model parameters calibrated using FLUXCOM.*

Vegetation class	λ	α	β	SW_{down0}	η_{vg}	$T_{s,vg}$		$M_{s,vg}$		R_{vg}	
						a_T	b_T	a_M	b_M	a_R	b_R
Grassland	0.1334	0.0269	0	157	3.2945	-0.0023	0.0004	2790.4	1320.2	3.96	2.9
Cropland	0.1209	0.0043	0	646	1.6002	-0.0008	-0.001	8588.3	7835.9	0.20	0.094
Savanna	0.1141	0.0049	0	682	3.7301	-0.0009	-0.003	10321.2	9546.6	-0.07	-0.01
Shrubland	0.0874	0.0239	0	303	3.3241	-0.001	0.002	5059.4	2749.0	0.72	0.4
Deciduous forest	0.2555	0.3422	0	206	2.4613	-0.043	-0.043	29429	29429	2.502	2.502
Evergreen forest	0.1729	0.3258	0	324	1.788	0.005	-0.003	4505.6	6906.2	0.44	0.4
Mixed Forest	0.2101	0.1601	0	501	2.3238	-0.005	-0.01	10214.6	10469.6	0.31	0.3

*Units are as follows: λ :µmol CO_2 m^{-2} s^{-1}/ µmol SW_{down} m^{-2} s^{-1}; α: µmol CO_2 m^{-2} s^{-1}/°C; β: µmol CO_2 m^{-2} s^{-1}; SW_{down0}: µmol m^{-2} s^{-1}; $T_{s,vg}$: µmol CO_2 m^{-2} s^{-1} K^{-1}; $M_{s,vg}$: µmol CO_2 m^{-2} s^{-1} m^{-3} m^3; η_{vg} and R_{vg}: dimensionless.

https://doi.org/10.5194/egusphere-2023-817
Preprint. Discussion started: 4 May 2023

Table 3: Spatial and temporal resolutions of the 14 dynamic global vegetation models from TRENDY. The annual NEE and GPP fluxes of India from individual models, calculated as the cumulative sum of corresponding fluxes at the models' original resolution in Pg C yr^{1} are also given.

Model	Spatial resolution	Temporal resolution	Reference	NEE (Pg C yr^{-1})	GPP (Pg C yr^{-1})
ISBA-CTRIP	1°×1°	Monthly	(Decharme et al., 2019)	-0.47	3.7
SDVGM	0.5°×0.5°	Monthly	(Woodward et al., 1995)	-0.14	2.7
IBIS	1°×1°	Monthly	(Foley et al., 2003; Kucharik et al., 2000)	-0.05	2.9
VISIT	0.5°×0.5°	Monthly	(Kato et al., 2013)	-0.21	2.9
CABLE-POP	1°×1°	Monthly	(Haverd et al., 2013)	-0.007	2.7
ORCHIDEEv	0.5°×0.5°	Monthly	(Lurton et al.,	-0.34	3.1

https://doi.org/10.5194/egusphere-2023-817
Preprint. Discussion started: 4 May 2023

3			2020)		
CLM5.0	1.25°╳0.942°	Monthly	(Buzan et al., 2015)	-0.24	2.1
DLEM	0.5°╳0.5°	Monthly	(Tian et al., 2015)	-0.45	3.5
ISAM	0.5°╳0.5°	Monthly	(Meiyappan et al., 2015)	-0.06	2.2
JSBACH	1.875°╳1.875°	Monthly	(Goll et al., 2015); (Reick et al., 2013)	-0.21	4.5
LPX-Bern	0.5°╳0.5°	Monthly	(Spahni et al., 2013; Stocker et al., 2013)	-0.07	2.9
OCN	1°╳1°	Monthly	(Zaehle & Friend, 2010)	-0.12	3.5
ORCHIDEE	0.5°╳0.5°	Monthly	(Krinner et al., 2005)	-0.32	2.6
LPJ	0.5°╳0.5°	Monthly	(Sitch et al., 2003)	-0.05	2.6

749

https://doi.org/10.5194/egusphere-2023-817
Preprint. Discussion started: 4 May 2023

Table 4: An overview of the eddy flux tower site, Betul.

Site Name	Sukhwan, Betul
Country	India
State	Madhya Pradesh
Location	21°51’46.84” N, 77°25’33.67” E
Area	1.76 km^2
Vegetation type	Deciduous forest
Canopy height	22 m
Tower height	34 m
Annual precipitation	1016 mm
Mean air temperature	27 °C
Dominant species	Tectona grandis, Miliusa tomentosa

https://doi.org/10.5194/egusphere-2023-817
Preprint. Discussion started: 4 May 2023

Table 5: Biome-specific scalars used for the conversion of TROPOSIF to $GPP_{TROPOSIF}$ across different vegetation classes (see Sect. 2.2).

Vegetation	$\gamma_{TROPOSIF,vg}$ (mW m^{-2} sr^{-1} nm^{-1})/ (µmol m^{-2} s^{-1})	$C_{TROPOSIF,vg}$
Grassland	7.84	0.40
Cropland	4.81	0.22
Savanna	5.12	0.32
Shrubland	5.00	0.39
Deciduous forest	5.35	0.34
Evergreen forest	5.47	0.64
Mixed forest	5.59	0.61

https://doi.org/10.5194/egusphere-2023-817
Preprint. Discussion started: 4 May 2023

Table 6: Comparison of monthly averaged NEE, GPP and R_{eco} fluxes from VPRM model simulations against EC observations for Betul from 2012 to 2018. Also reporting values for 2018, the only common year for which the SIF, and EC data are available.

Model vs Observations	2012 - 2018 (μmol m^{-2} s^{-1})			2018		
	R^2	RMSE	MBE	R^2	RMSE	MBE
			GPP			
$VPRM_{STD}$	0.71	8.3	-6.7	0.74	8	6.2
$VPRM_{GOSIF}$	0.71	4.9	-3.4	0.74	4.1	2.57
$VPRM_{TROPOSIF}$	0.71	4.3	-2.6	0.74	3.6	1.77
			R_{eco}			
$VPRM_{STD}$	0.02	5.7	-3.5	0.01	4.9	-2.9
$VPRM_{ST}$	0.06	4.4	0.08	0.16	3.8	0.7

https://doi.org/10.5194/egusphere-2023-817
Preprint. Discussion started: 4 May 2023

$VPRM_{SM}$	0.80	2.0	-0.01	0.84	1.6	0.4
$VPRM_{MOD(STSM)}$	0.82	1.9	-0.01	0.88	1.4	0.2
			NEE			
$VPRM_{STD}$ (-GPP $_{(VPRMSTD)}$ + $R_{eco(VPRMSTD)}$)	0.59	4.4	3.2	0.65	5.2	3.3
$VPRM_{GOSIF,SMST}$ (-GPP$_{(VPRMGOSIF)}$+ $R_{eco(VPRMMOD(STSM))}$)	0.53	4.4	3.2	0.66	4.3	2.8
$VPRM_{TROPOSIF,SMST}$ (-GPP$_{(VPRMTROPOSIF)}$+ $R_{eco(VPRMMOD(STSM))}$)	0.56	3.8	2.4	0.68	3.7	2
TRENDY	0.45	3.3	1.1	0.51	3.6	1.4
CT	0.24	3.5	1.2	0.17	4	1.4

767

https://doi.org/10.5194/egusphere-2023-817
Preprint. Discussion started: 4 May 2023

Table 7. Biome specific annual fluxes from $VPRM_{refined}$ in kg C m^{-2} yr^{-1} and total fluxes in Pg C yr^{-1} are provided for the year 2020. The reported NEE values used respiration model parameters calibrated using FLUXNET.

Statistics for the year 2020								
		Grassland	Cropland	Savanna	Shrubland	Evergreen Forest	Mixed Forest	Deciduous Forest
NEE	kg C m^{-2} yr^{-1}	0.11	-0.28	-1.31	-0.39	-2.42	-2.65	2.70
	Pg C yr^{-1}	0.005	-0.30	-0.01	-0.07	-0.31	-0.22	0.31
GPP	kg C m^{-2} yr^{-1}	0.66	1.43	4.60	1.74	5.51	6.35	4.63
	Pg C yr^{-1}	0.03	2.60	0.062	0.63	0.78	0.64	0.49
R_{eco}	kg C m^{-2} yr^{-1}	0.69	1.19	2.92	1.35	3.05	3.4	5.71
	Pg C Yr^{-1}	0.03	2.21	0.04	0.51	0.36	0.32	0.66

https://doi.org/10.5194/egusphere-2023-817
Preprint. Discussion started: 4 May 2023

774 # Figures

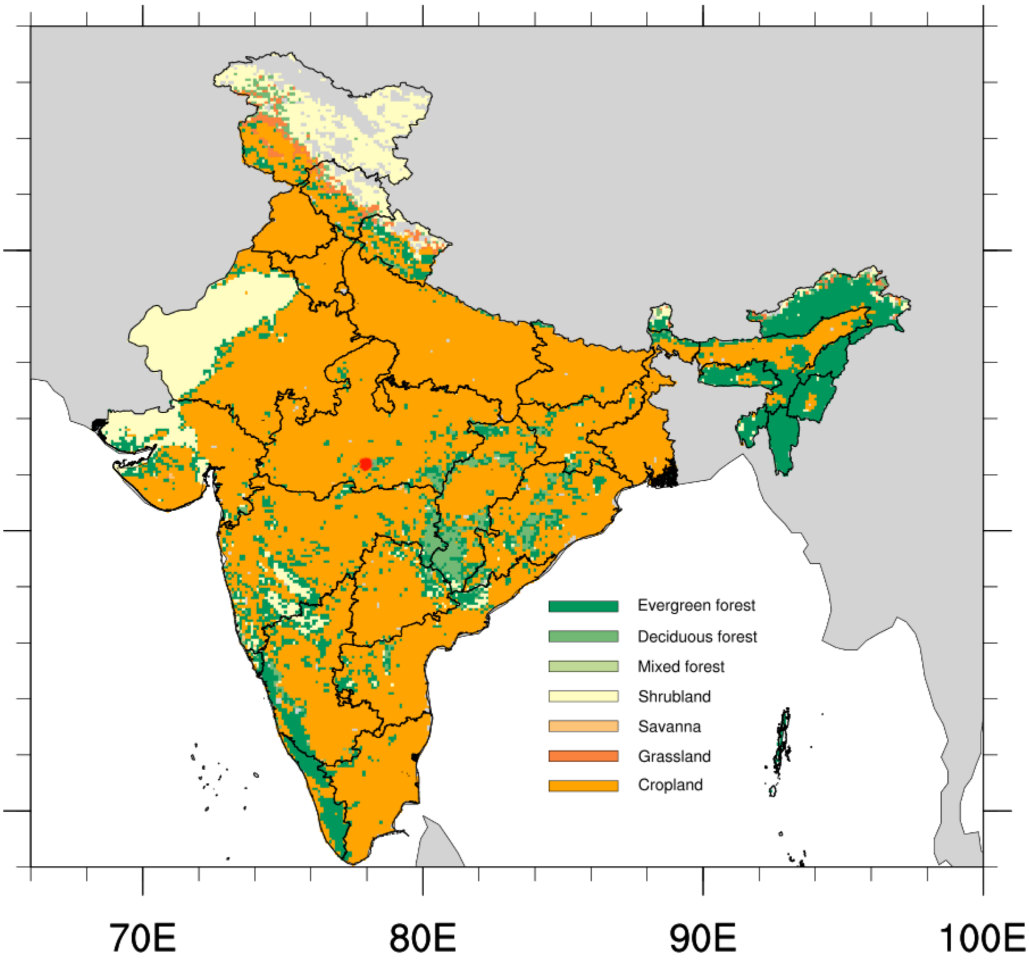

775

776 **Fig. 1: An overview of the major vegetation classes for the study region. Solid red circle**
777 **denotes the Eddy covariance observation site at Betul.**

https://doi.org/10.5194/egusphere-2023-817
Preprint. Discussion started: 4 May 2023

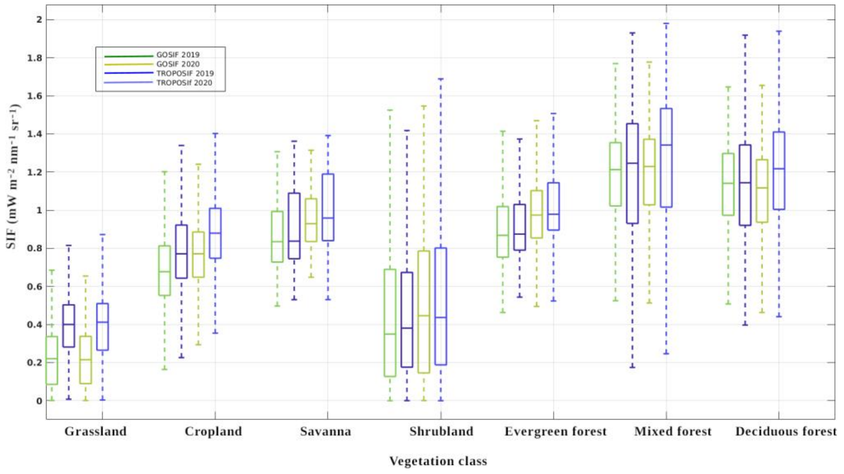

Fig. 2: Comparison between annually averaged SIF retrievals from OCO-2 (GOSIF) and TROPOSIF based products across vegetation classes over India for 2019. GOSIF (estimated at 757 nm) are scaled by respective biome-specific scaling factors (see Table. 5) to compare with TROPOMI SIF (estimated at 757 nm and 771 nm).

https://doi.org/10.5194/egusphere-2023-817
Preprint. Discussion started: 4 May 2023

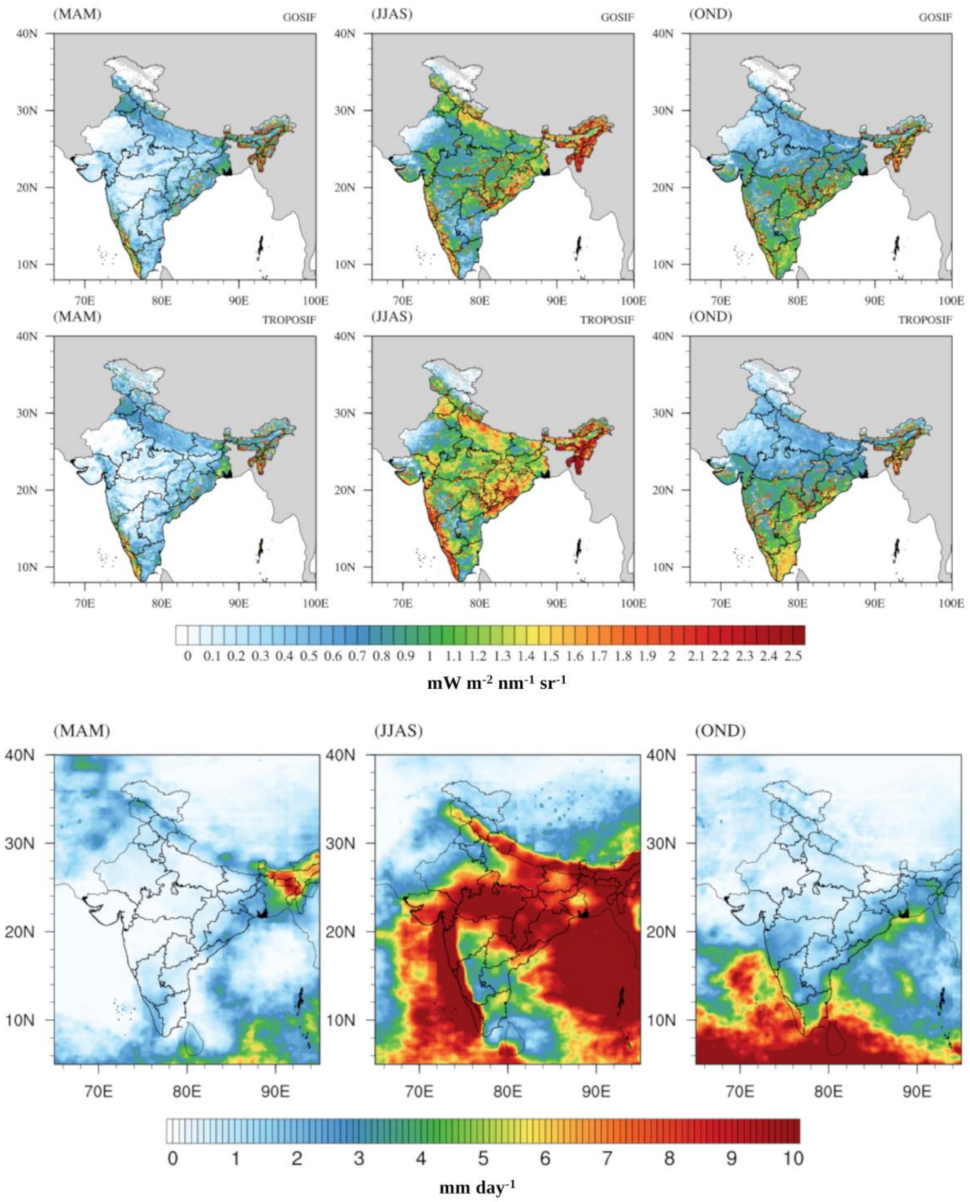

Fig. 3: Seasonal distribution patterns of SIF and precipitation over India for the year 2019: First row: GOSIF, Second row: TROPOSIF, and Third row: TRMM precipitation data, respectively.

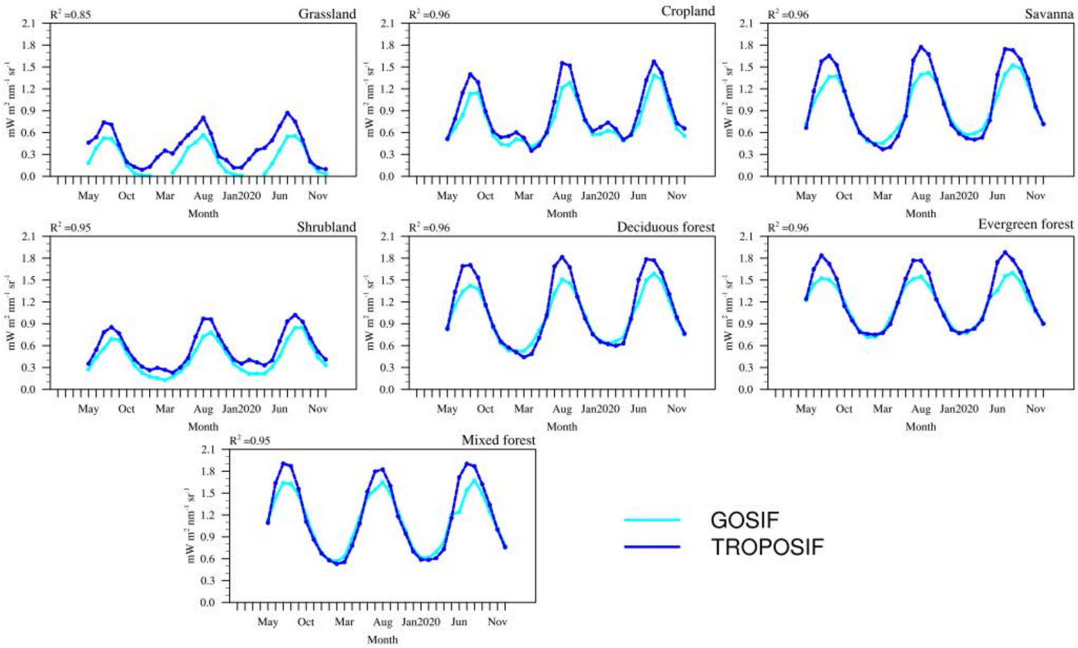

Fig. 4: Time series of monthly averaged SIF (GOSIF and TROPOSIF) across different biomes over India from 2018 to 2020. The vegetation classification based on SYNMAP is used to represent SIF for different biomes.

https://doi.org/10.5194/egusphere-2023-817
Preprint. Discussion started: 4 May 2023

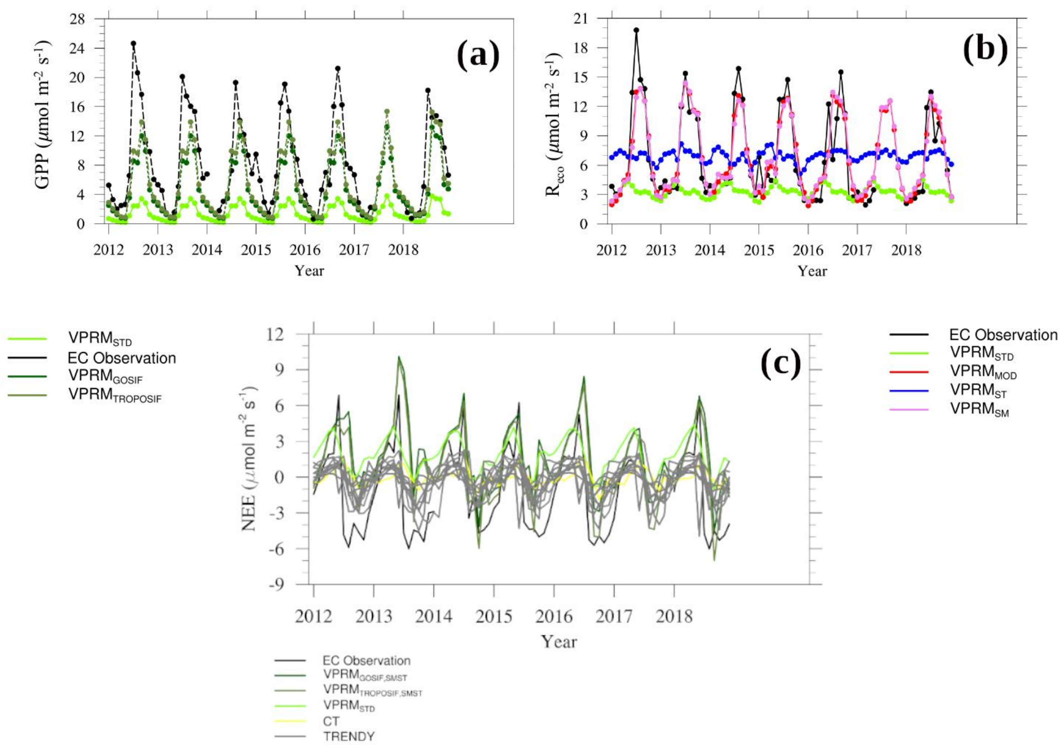

Fig. 5: Comparison of monthly averaged EC observations with a) GPP, b) R_{eco}, and c) NEE simulations over Betul for the period 2012 to 2018.

https://doi.org/10.5194/egusphere-2023-817
Preprint. Discussion started: 4 May 2023

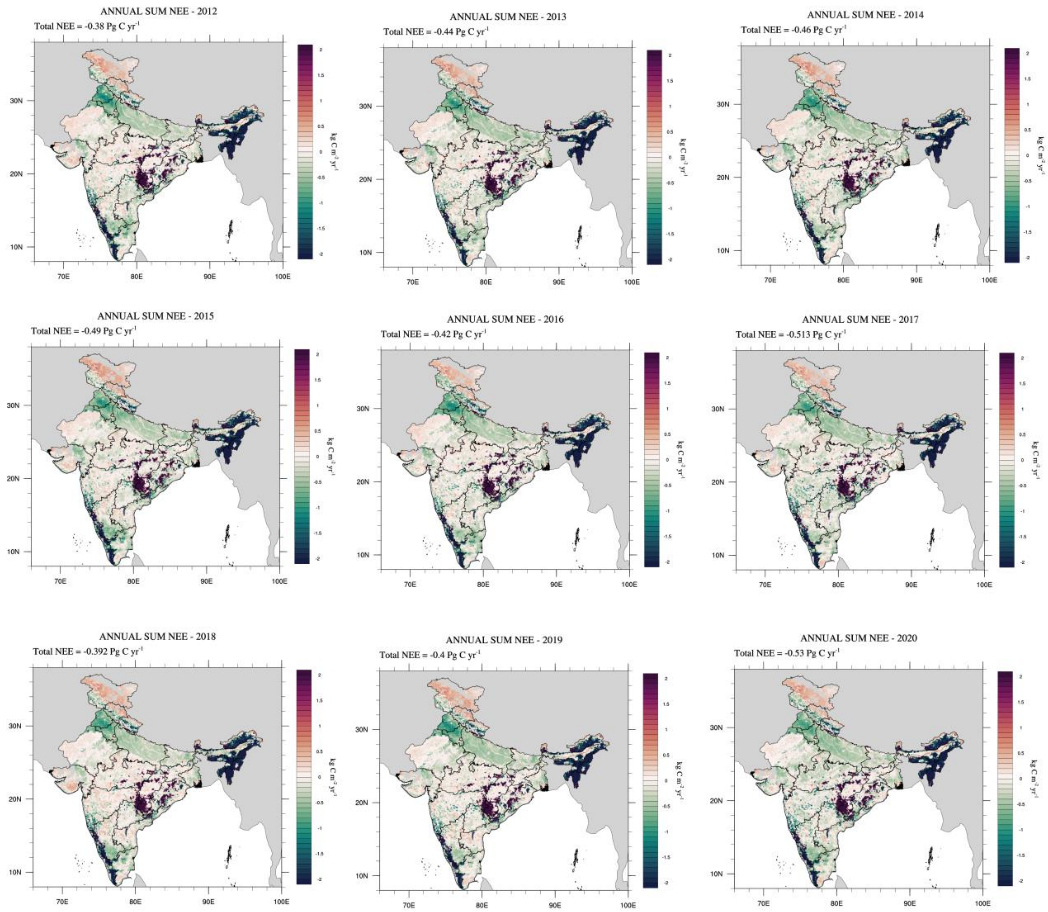

Fig. 6: Spatial patterns in annual NEE fluxes as simulated by VPRM$_{refined}$ over the Indian region for the years from 2012 to 2020. The shown NEE values used respiration model parameters calibrated using FLUXNET.

https://doi.org/10.5194/egusphere-2023-817
Preprint. Discussion started: 4 May 2023

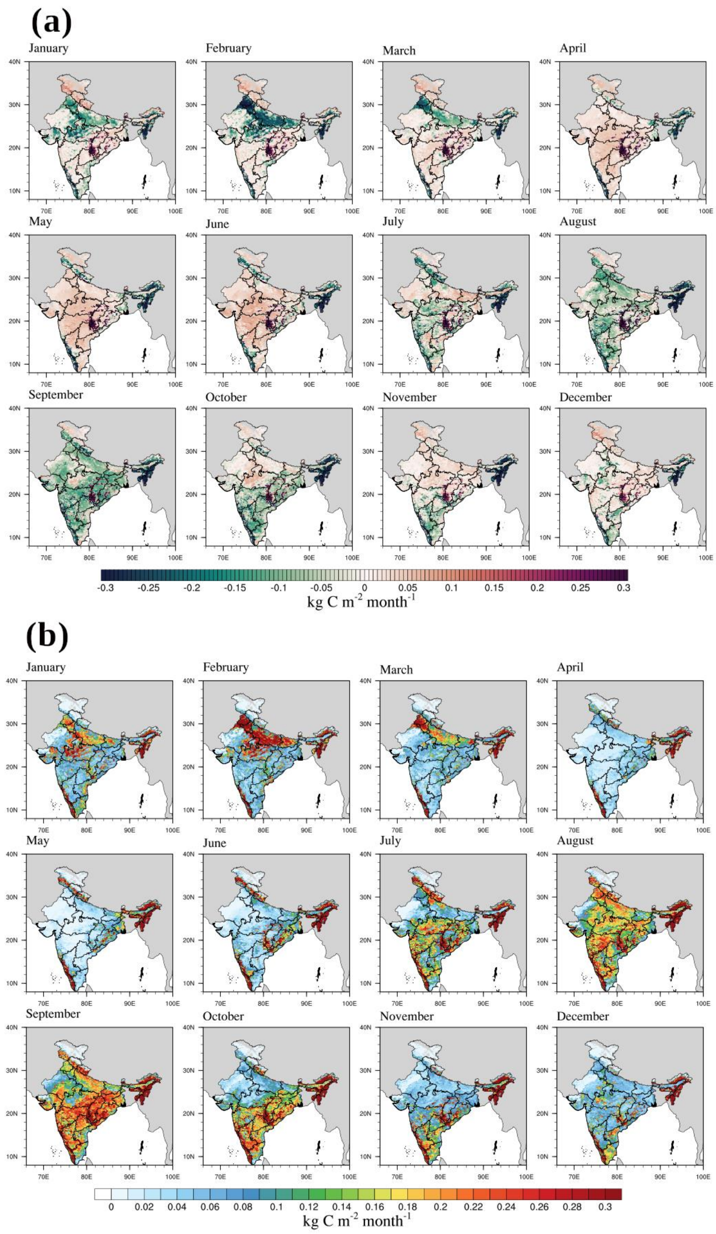

Fig. 7: Spatial pattern in monthly averaged fluxes from VPRM$_{\text{refined}}$ for the year 2020. a) NEE and b) GPP. The shown NEE values used respiration model parameters calibrated using FLUXNET.

https://doi.org/10.5194/egusphere-2023-817
Preprint. Discussion started: 4 May 2023

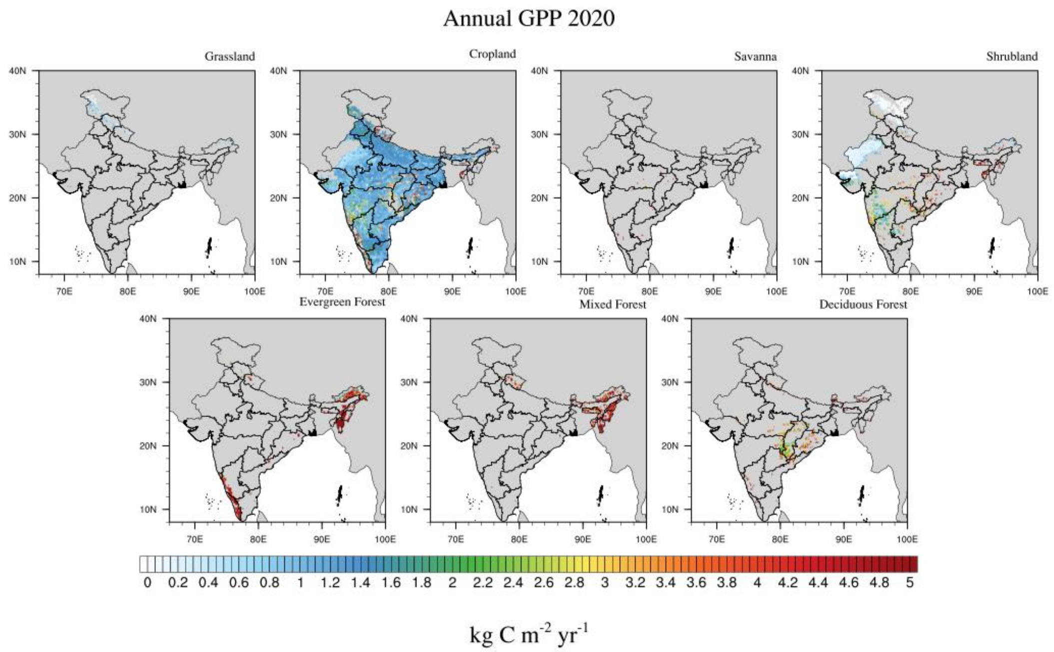

802

803 **Fig. 8: Spatial pattern in the annual GPP from $VPRM_{refined}$ over different vegetation for the**

804 **year 2020.**

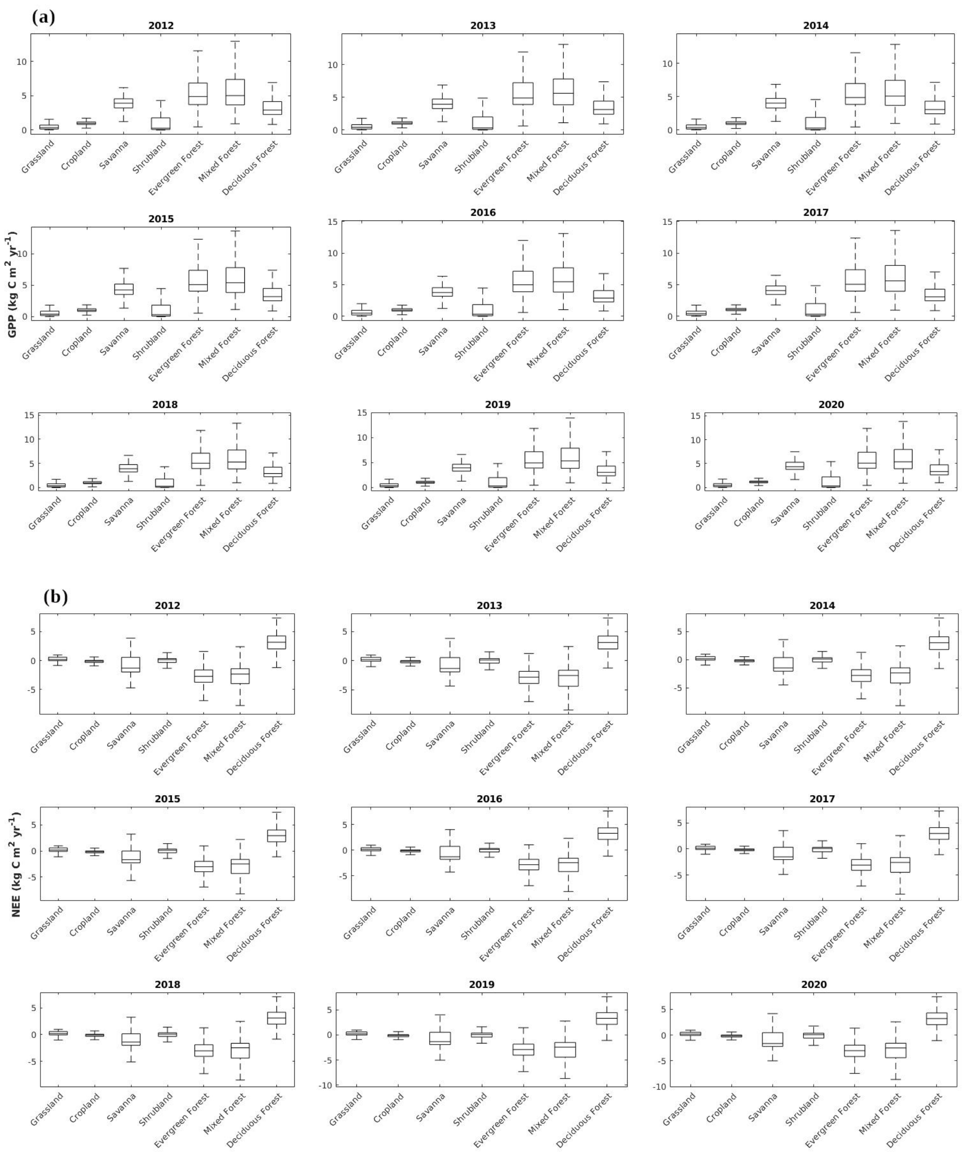

Fig. 9: The biome-specific annual VPRM$_{refined}$ a) GPP and b) NEE from 2012 to 2020. Upper and lower limit of the box shows 25th and 75th percentile of the data and center line shows the median. All the values which are 1.5 times higher than the 25th and 75th percentile are considered as outliers and are removed from the graph. The shown NEE values used respiration model parameters calibrated using FLUXNET.

https://doi.org/10.5194/egusphere-2023-817
Preprint. Discussion started: 4 May 2023

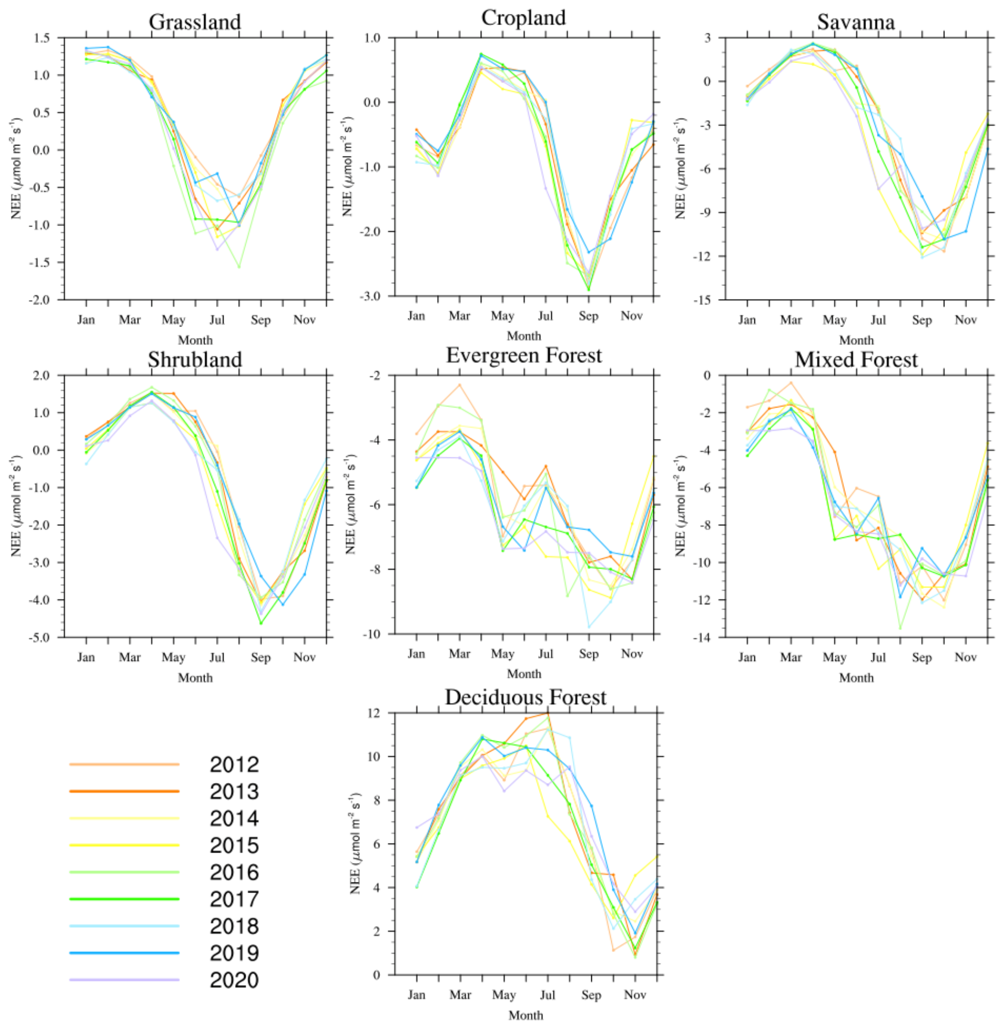

Fig. 10: Temporal variations in monthly averaged NEE fluxes from VPRM$_{refined}$ for the years 2012 to 2020. The shown NEE values used respiration model parameters calibrated using FLUXNET.

https://doi.org/10.5194/egusphere-2023-817
Preprint. Discussion started: 4 May 2023

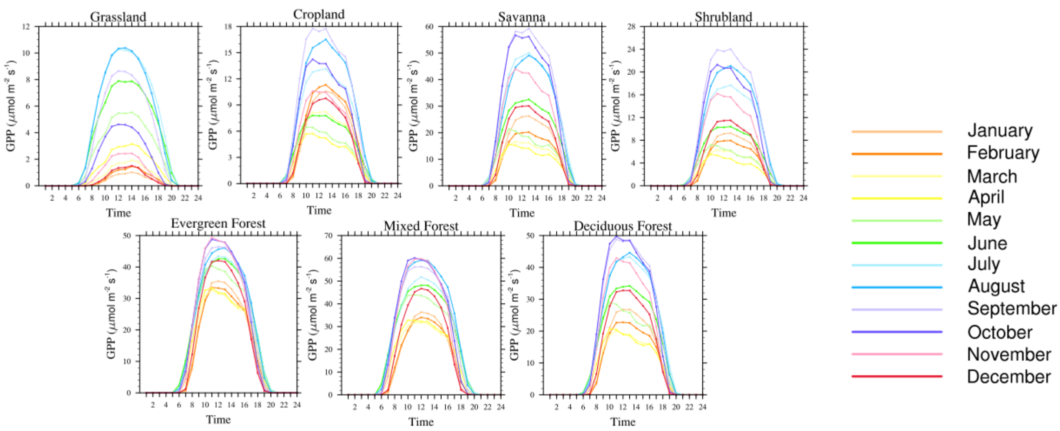

Fig. 11: Diurnal variations in $VPRM_{refined}$ GPP fluxes during 2020.

https://doi.org/10.5194/egusphere-2023-817
Preprint. Discussion started: 4 May 2023

References:

Albright, R., Corbett, A., Jiang, X., Creecy, E., Newman, S., Li, K., Liang, M., and Yung, Y. L.: Seasonal Variations of Solar-Induced Fluorescence, Precipitation, and Carbon Dioxide Over the Amazon, Earth Space Sci., 9, https://doi.org/10.1029/2021EA002078, 2022.

Baldocchi, D., Falge, E., Gu, L., Olson, R., Hollinger, D., Running, S., Anthoni, P., Bernhofer, C., Davis, K., Evans, R., Fuentes, J., Goldstein, A., Katul, G., Law, B., Lee, X., Malhi, Y., Meyers, T., Munger, W., Oechel, W., Paw, K. T., Pilegaard, K., Schmid, H. P., Valentini, R., Verma, S., Vesala, T., Wilson, K., and Wofsy, S.: FLUXNET: A New Tool to Study the Temporal and Spatial Variability of Ecosystem–Scale Carbon Dioxide, Water Vapor, and Energy Flux Densities, Bull. Am. Meteorol. Soc., 82, 2415–2434, https://doi.org/10.1175/1520-0477(2001)082<2415:FANTTS>2.3.CO;2, 2001.

Botía, S., Komiya, S., Marshall, J., Koch, T., Gałkowski, M., Lavric, J., Gomes-Alves, E., Walter, D., Fisch, G., Pinho, D. M., Nelson, B. W., Martins, G., Luijkx, I. T., Koren, G., Florentie, L., Carioca de Araújo, A., Sá, M., Andreae, M. O., Heimann, M., Peters, W., and Gerbig, C.: The CO_2 record at the Amazon Tall Tower Observatory: A new opportunity to study processes on seasonal and inter-annual scales, Glob. Change Biol., 28, 588–611, https://doi.org/10.1111/gcb.15905, 2022.

Buzan, J. R., Oleson, K., and Huber, M.: Implementation and comparison of a suite of heat stress metrics within the Community Land Model version 4.5, Geosci. Model Dev., 8, 151–170, https://doi.org/10.5194/gmd-8-151-2015, 2015.

Cervarich, M., Shu, S., Jain, A. K., Arneth, A., Canadell, J., Friedlingstein, P., Houghton, R. A., Kato, E., Koven, C., Patra, P., Poulter, B., Sitch, S., Stocker, B., Viovy, N., Wiltshire, A., and Zeng, N.: The terrestrial carbon budget of South and Southeast Asia, Environ. Res. Lett., 11, 105006, https://doi.org/10.1088/1748-9326/11/10/105006, 2016.

https://doi.org/10.5194/egusphere-2023-817
Preprint. Discussion started: 4 May 2023

Chen, F., Manning, K. W., LeMone, M. A., Trier, S. B., Alfieri, J. G., Roberts, R., Tewari, M., Niyogi, D., Horst, T. W., Oncley, S. P., Basara, J. B., and Blanken, P. D.: Description and Evaluation of the Characteristics of the NCAR High-Resolution Land Data Assimilation System, J. Appl. Meteorol. Climatol., 46, 694–713, https://doi.org/10.1175/JAM2463.1, 2007.

Copernicus Climate Change Service: ERA5-Land hourly data from 2001 to present, https://doi.org/10.24381/CDS.E2161BAC, 2019.

Dadhwal, V. K.: ASSESSMENT OF INDIAN CARBON CYCLE COMPONENTS USING EARTH OBSERVATION SYSTEMS AND GROUND INVENTORY, Int. Arch. Photogramm. Remote Sens. Spat. Inf. Sci., XXXIX-B8, 249–254, https://doi.org/10.5194/isprsarchives-XXXIX-B8-249-2012, 2012.

Dayalu, A., Munger, W., Wofsy, S. C., Wang, Y., Nehrkorn, T., Zhao, Y., McElroy, M. B., Nielsen, C., and Luus, K.: VPRM-CHINA: Using the Vegetation, Photosynthesis, and Respiration Model to partition contributions to CO2 measurements in Northern China during the 2005–2009 growing seasons, Biogeochemistry: Air - Land Exchange, https://doi.org/10.5194/bg-2017-504, 2017.

Deb Burman, P. K., Launiainen, S., Mukherjee, S., Chakraborty, S., Gogoi, N., Murkute, C., Lohani, P., Sarma, D., and Kumar, K.: Ecosystem-atmosphere carbon and water exchanges of subtropical evergreen and deciduous forests in India, For. Ecol. Manag., 495, 119371, https://doi.org/10.1016/j.foreco.2021.119371, 2021.

Decharme, B., Delire, C., Minvielle, M., Colin, J., Vergnes, J., Alias, A., Saint-Martin, D., Séférian, R., Sénési, S., and Voldoire, A.: Recent Changes in the ISBA-CTRIP Land Surface System for Use in the CNRM-CM6 Climate Model and in Global Off-Line Hydrological Applications, J. Adv. Model. Earth Syst., 11, 1207–1252, https://doi.org/10.1029/2018MS001545, 2019.

https://doi.org/10.5194/egusphere-2023-817
Preprint. Discussion started: 4 May 2023

Dee, D. P., Uppala, S. M., Simmons, A. J., Berrisford, P., Poli, P., Kobayashi, S., Andrae, U., Balmaseda, M. A., Balsamo, G., Bauer, P., Bechtold, P., Beljaars, A. C. M., van de Berg, L., Bidlot, J., Bormann, N., Delsol, C., Dragani, R., Fuentes, M., Geer, A. J., Haimberger, L., Healy, S. B., Hersbach, H., Hólm, E. V., Isaksen, L., Kållberg, P., Köhler, M., Matricardi, M., McNally, A. P., Monge-Sanz, B. M., Morcrette, J.-J., Park, B.-K., Peubey, C., de Rosnay, P., Tavolato, C., Thépaut, J.-N., and Vitart, F.: The ERA-Interim reanalysis: configuration and performance of the data assimilation system, Q. J. R. Meteorol. Soc., 137, 553–597, https://doi.org/10.1002/qj.828, 2011.

Flexas, J., Bota, J., Galmés, J., Medrano, H., and Ribas-Carbó, M.: Keeping a positive carbon balance under adverse conditions: responses of photosynthesis and respiration to water stress, Physiol. Plant., 127, 343–352, https://doi.org/10.1111/j.1399-3054.2006.00621.x, 2006.

Foley, J. A., Coe, M. T., Scheffer, M., and Wang, G.: Regime Shifts in the Sahara and Sahel: Interactions between Ecological and Climatic Systems in Northern Africa, Ecosystems, 6, 524–532, https://doi.org/10.1007/s10021-002-0227-0, 2003.

Frankenberg, C., Fisher, J. B., Lee, J., Guanter, L., Van der Tol, C., Toon, G. C., kuze, A., Yokota, T., Badgley, G. M., Butz, A., Jung, M., Saatchi, S. S., and Worden, J.: New global observations of the terrestrial carbon cycle from GOSAT: Patterns of vegetation fluorescence with gross primary productivity, 2011, A41H-02, 2011.

Friedlingstein, P., O'Sullivan, M., Jones, M. W., Andrew, R. M., Gregor, L., Hauck, J., Le Quéré, C., Luijkx, I. T., Olsen, A., Peters, G. P., Peters, W., Pongratz, J., Schwingshackl, C., Sitch, S., Canadell, J. G., Ciais, P., Jackson, R. B., Alin, S. R., Alkama, R., Arneth, A., Arora, V. K., Bates, N. R., Becker, M., Bellouin, N., Bittig, H. C., Bopp, L., Chevallier, F., Chini, L. P., Cronin, M., Evans, W., Falk, S., Feely, R. A., Gasser, T., Gehlen, M., Gkritzalis, T., Gloege, L., Grassi, G., Gruber, N., Gürses, Ö., Harris, I., Hefner, M., Houghton, R. A., Hurtt, G. C., Iida, Y., Ilyina, T.,

https://doi.org/10.5194/egusphere-2023-817
Preprint. Discussion started: 4 May 2023

Jain, A. K., Jersild, A., Kadono, K., Kato, E., Kennedy, D., Klein Goldewijk, K., Knauer, J., Korsbakken, J. I., Landschützer, P., Lefèvre, N., Lindsay, K., Liu, J., Liu, Z., Marland, G., Mayot, N., McGrath, M. J., Metzl, N., Monacci, N. M., Munro, D. R., Nakaoka, S.-I., Niwa, Y., O'Brien, K., Ono, T., Palmer, P. I., Pan, N., Pierrot, D., Pocock, K., Poulter, B., Resplandy, L., Robertson, E., Rödenbeck, C., Rodriguez, C., Rosan, T. M., Schwinger, J., Séférian, R., Shutler, J. D., Skjelvan, I., Steinhoff, T., Sun, Q., Sutton, A. J., Sweeney, C., Takao, S., Tanhua, T., Tans, P. P., Tian, X., Tian, H., Tilbrook, B., Tsujino, H., Tubiello, F., van der Werf, G. R., Walker, A. P., Wanninkhof, R., Whitehead, C., Willstrand Wranne, A., et al.: Global Carbon Budget 2022, Earth Syst. Sci. Data, 14, 4811–4900, https://doi.org/10.5194/essd-14-4811-2022, 2022.

Gamon, J. A., Field, C. B., Goulden, M. L., Griffin, K. L., Hartley, A. E., Joel, G., Penuelas, J., and Valentini, R.: Relationships Between NDVI, Canopy Structure, and Photosynthesis in Three Californian Vegetation Types, Ecol. Appl., 5, 28–41, https://doi.org/10.2307/1942049, 1995.

Goll, D. S., Brovkin, V., Liski, J., Raddatz, T., Thum, T., and Todd-Brown, K. E. O.: Strong dependence of CO_2 emissions from anthropogenic land cover change on initial land cover and soil carbon parametrization, Glob. Biogeochem. Cycles, 29, 1511–1523, https://doi.org/10.1002/2014GB004988, 2015.

Goroshi, S. K., Singh, R. P., Pradhan, R., and Parihar, J. S.: Assessment of net primary productivity over India using Indian geostationary satellite (INSAT-3A) data, Int. Arch. Photogramm. Remote Sens. Spat. Inf. Sci., XL–8, 561–568, https://doi.org/10.5194/isprsarchives-XL-8-561-2014, 2014.

Gourdji, S. M., Karion, A., Lopez-Coto, I., Ghosh, S., Mueller, K. L., Zhou, Y., Williams, C. A., Baker, I. T., Haynes, K. D., and Whetstone, J. R.: A Modified Vegetation Photosynthesis and Respiration Model (VPRM) for the Eastern USA and Canada, Evaluated With Comparison to

https://doi.org/10.5194/egusphere-2023-817
Preprint. Discussion started: 4 May 2023

Atmospheric Observations and Other Biospheric Models, J. Geophys. Res. Biogeosciences, 127, https://doi.org/10.1029/2021JG006290, 2022.

Gu, L., Han, J., Wood, J. D., Chang, C. Y., and Sun, Y.: Sun-induced Chl fluorescence and its importance for biophysical modeling of photosynthesis based on light reactions, New Phytol., 223, 1179–1191, https://doi.org/10.1111/nph.15796, 2019.

Guanter, L., Bacour, C., Schneider, A., Aben, I., van Kempen, T. A., Maignan, F., Retscher, C., Köhler, P., Frankenberg, C., Joiner, J., and Zhang, Y.: The TROPOSIF global sun-induced fluorescence dataset from the Sentinel-5P TROPOMI mission, Earth Syst. Sci. Data, 13, 5423–5440, https://doi.org/10.5194/essd-13-5423-2021, 2021.

Han, G., Sun, B., Chu, X., Xing, Q., Song, W., and Xia, J.: Precipitation events reduce soil respiration in a coastal wetland based on four-year continuous field measurements, Agric. For. Meteorol., 256–257, 292–303, https://doi.org/10.1016/j.agrformet.2018.03.018, 2018.

Haverd, V., Smith, B., Cook, G. D., Briggs, P. R., Nieradzik, L., Roxburgh, S. H., Liedloff, A., Meyer, C. P., and Canadell, J. G.: A stand-alone tree demography and landscape structure module for Earth system models, Geophys. Res. Lett., 40, 5234–5239, https://doi.org/10.1002/grl.50972, 2013.

Hersbach, H., Bell, B., Berrisford, P., Hirahara, S., Horányi, A., Muñoz-Sabater, J., Nicolas, J., Peubey, C., Radu, R., Schepers, D., Simmons, A., Soci, C., Abdalla, S., Abellan, X., Balsamo, G., Bechtold, P., Biavati, G., Bidlot, J., Bonavita, M., Chiara, G., Dahlgren, P., Dee, D., Diamantakis, M., Dragani, R., Flemming, J., Forbes, R., Fuentes, M., Geer, A., Haimberger, L., Healy, S., Hogan, R. J., Hólm, E., Janisková, M., Keeley, S., Laloyaux, P., Lopez, P., Lupu, C., Radnoti, G., Rosnay, P., Rozum, I., Vamborg, F., Villaume, S., and Thépaut, J.: The ERA5 global reanalysis, Q. J. R. Meteorol. Soc., 146, 1999–2049, https://doi.org/10.1002/qj.3803, 2020.

https://doi.org/10.5194/egusphere-2023-817
Preprint. Discussion started: 4 May 2023

Jha, C. S., Thumaty, K. C., Rodda, S. R., Sonakia, A., and Dadhwal, V. K.: Analysis of carbon dioxide, water vapour and energy fluxes over an Indian teak mixed deciduous forest for winter and summer months using eddy covariance technique, J. Earth Syst. Sci., 122, 1259–1268, https://doi.org/10.1007/s12040-013-0350-7, 2013.

Joiner, J., Yoshida, Y., Guanter, L., and Middleton, E. M.: New methods for the retrieval of chlorophyll red fluorescence from hyperspectral satellite instruments: simulations andapplication to GOME-2 and SCIAMACHY, Atmospheric Meas. Tech., 9, 3939–3967, https://doi.org/10.5194/amt-9-3939-2016, 2016.

Joiner, J., Yoshida, Y., Zhang, Y., Duveiller, G., Jung, M., Lyapustin, A., Wang, Y., and Tucker, C.: Estimation of Terrestrial Global Gross Primary Production (GPP) with Satellite Data-Driven Models and Eddy Covariance Flux Data, Remote Sens., 10, 1346, https://doi.org/10.3390/rs10091346, 2018.

Jung, M., Henkel, K., Herold, M., and Churkina, G.: Exploiting synergies of global land cover products for carbon cycle modeling, Remote Sens. Environ., 101, 534–553, https://doi.org/10.1016/j.rse.2006.01.020, 2006.

Jung, M., Schwalm, C., Migliavacca, M., Walther, S., Camps-Valls, G., Koirala, S., Anthoni, P., Besnard, S., Bodesheim, P., Carvalhais, N., Chevallier, F., Gans, F., Goll, D. S., Haverd, V., Köhler, P., Ichii, K., Jain, A. K., Liu, J., Lombardozzi, D., Nabel, J. E. M. S., Nelson, J. A., O'Sullivan, M., Pallandt, M., Papale, D., Peters, W., Pongratz, J., Rödenbeck, C., Sitch, S., Tramontana, G., Walker, A., Weber, U., and Reichstein, M.: Scaling carbon fluxes from eddy covariance sites to globe: synthesis and evaluation of the FLUXCOM approach, Biogeosciences, 17, 1343–1365, https://doi.org/10.5194/bg-17-1343-2020, 2020.

https://doi.org/10.5194/egusphere-2023-817
Preprint. Discussion started: 4 May 2023

Kato, E., Kinoshita, T., Ito, A., Kawamiya, M., and Yamagata, Y.: Evaluation of spatially explicit emission scenario of land-use change and biomass burning using a process-based biogeochemical model, J. Land Use Sci., 8, 104–122, https://doi.org/10.1080/1747423X.2011.628705, 2013.

Köhler, P., Guanter, L., and Joiner, J.: A linear method for the retrieval of sun-induced chlorophyll fluorescence from GOME-2 and SCIAMACHY data, Atmospheric Meas. Tech., 8, 2589–2608, https://doi.org/10.5194/amt-8-2589-2015, 2015.

Köhler, P., Frankenberg, C., Magney, T. S., Guanter, L., Joiner, J., and Landgraf, J.: Global Retrievals of Solar-Induced Chlorophyll Fluorescence With TROPOMI: First Results and Intersensor Comparison to OCO-2, Geophys. Res. Lett., 45, https://doi.org/10.1029/2018GL079031, 2018.

Krinner, G., Viovy, N., de Noblet-Ducoudré, N., Ogée, J., Polcher, J., Friedlingstein, P., Ciais, P., Sitch, S., and Prentice, I. C.: A dynamic global vegetation model for studies of the coupled atmosphere-biosphere system: DVGM FOR COUPLED CLIMATE STUDIES, Glob. Biogeochem. Cycles, 19, https://doi.org/10.1029/2003GB002199, 2005.

Kucharik, C. J., Foley, J. A., Delire, C., Fisher, V. A., Coe, M. T., Lenters, J. D., Young-Molling, C., Ramankutty, N., Norman, J. M., and Gower, S. T.: Testing the performance of a dynamic global ecosystem model: Water balance, carbon balance, and vegetation structure, Glob. Biogeochem. Cycles, 14, 795–825, https://doi.org/10.1029/1999GB001138, 2000.

Kummerow, C., Simpson, J., Thiele, O., Barnes, W., Chang, A. T. C., Stocker, E., Adler, R. F., Hou, A., Kakar, R., Wentz, F., Ashcroft, P., Kozu, T., Hong, Y., Okamoto, K., Iguchi, T., Kuroiwa, H., Im, E., Haddad, Z., Huffman, G., Ferrier, B., Olson, W. S., Zipser, E., Smith, E. A., Wilheit, T. T., North, G., Krishnamurti, T., and Nakamura, K.: The Status of the Tropical Rainfall Measuring Mission (TRMM) after Two Years in Orbit, J. Appl. Meteorol., 39, 1965–1982, https://doi.org/10.1175/1520-0450(2001)040<1965:TSOTTR>2.0.CO;2, 2000.

https://doi.org/10.5194/egusphere-2023-817
Preprint. Discussion started: 4 May 2023

Li and Xiao: Mapping Photosynthesis Solely from Solar-Induced Chlorophyll Fluorescence: A Global, Fine-Resolution Dataset of Gross Primary Production Derived from OCO-2, Remote Sens., 11, 2563, https://doi.org/10.3390/rs11212563, 2019a.

Li, X. and Xiao, J.: A Global, 0.05-Degree Product of Solar-Induced Chlorophyll Fluorescence Derived from OCO-2, MODIS, and Reanalysis Data, Remote Sens., 11, 517, https://doi.org/10.3390/rs11050517, 2019b.

Li, X., Xiao, J., He, B., Altaf Arain, M., Beringer, J., Desai, A. R., Emmel, C., Hollinger, D. Y., Krasnova, A., Mammarella, I., Noe, S. M., Ortiz, P. S., Rey-Sanchez, A. C., Rocha, A. V., and Varlagin, A.: Solar-induced chlorophyll fluorescence is strongly correlated with terrestrial photosynthesis for a wide variety of biomes: First global analysis based on OCO-2 and flux tower observations, Glob. Change Biol., 24, 3990–4008, https://doi.org/10.1111/gcb.14297, 2018.

Lurton, T., Balkanski, Y., Bastrikov, V., Bekki, S., Bopp, L., Braconnot, P., Brockmann, P., Cadule, P., Contoux, C., Cozic, A., Cugnet, D., Dufresne, J., Éthé, C., Foujols, M., Ghattas, J., Hauglustaine, D., Hu, R., Kageyama, M., Khodri, M., Lebas, N., Levavasseur, G., Marchand, M., Ottlé, C., Peylin, P., Sima, A., Szopa, S., Thiéblemont, R., Vuichard, N., and Boucher, O.: Implementation of the CMIP6 Forcing Data in the IPSL-CM6A-LR Model, J. Adv. Model. Earth Syst., 12, https://doi.org/10.1029/2019MS001940, 2020.

Luus, K. A. and Lin, J. C.: The Polar Vegetation Photosynthesis and Respiration Model: a parsimonious, satellite-data-driven model of high-latitude CO₂ exchange, Geosci. Model Dev., 8, 2655–2674, https://doi.org/10.5194/gmd-8-2655-2015, 2015.

Mahadevan, P., Wofsy, S. C., Matross, D. M., Xiao, X., Dunn, A. L., Lin, J. C., Gerbig, C., Munger, J. W., Chow, V. Y., and Gottlieb, E. W.: A satellite-based biosphere parameterization for net ecosystem CO_2 exchange: Vegetation Photosynthesis and Respiration Model (VPRM):

https://doi.org/10.5194/egusphere-2023-817
Preprint. Discussion started: 4 May 2023

NET ECOSYSTEM EXCHANGE MODEL, Glob. Biogeochem. Cycles, 22, n/a-n/a, https://doi.org/10.1029/2006GB002735, 2008.

Martens, B., Miralles, D. G., Lievens, H., van der Schalie, R., de Jeu, R. A. M., Fernández-Prieto, D., Beck, H. E., Dorigo, W. A., and Verhoest, N. E. C.: GLEAM v3: satellite-based land evaporation and root-zone soil moisture, Geosci. Model Dev., 10, 1903–1925, https://doi.org/10.5194/gmd-10-1903-2017, 2017.

Meir, P., Metcalfe, D. B., Costa, A. C. L., and Fisher, R. A.: The fate of assimilated carbon during drought: impacts on respiration in Amazon rainforests, Philos. Trans. R. Soc. B Biol. Sci., 363, 1849–1855, https://doi.org/10.1098/rstb.2007.0021, 2008.

Meiyappan, P., Jain, A. K., and House, J. I.: Increased influence of nitrogen limitation on CO_2 emissions from future land use and land use change, Glob. Biogeochem. Cycles, 29, 1524–1548, https://doi.org/10.1002/2015GB005086, 2015.

Michalak, A. M.: A geostatistical approach to surface flux estimation of atmospheric trace gases, J. Geophys. Res., 109, D14109, https://doi.org/10.1029/2003JD004422, 2004.

Molchanov, A. G.: Effect of moisture availability on photosynthetic productivity and autotrophic respiration of an oak stand, Russ. J. Plant Physiol., 56, 769–779, https://doi.org/10.1134/S1021443709060065, 2009.

Nayak, R. K., Patel, N. R., and Dadhwal, V. K.: Estimation and analysis of terrestrial net primary productivity over India by remote-sensing-driven terrestrial biosphere model, Environ. Monit. Assess., 170, 195–213, https://doi.org/10.1007/s10661-009-1226-9, 2010.

Nayak, R. K., Patel, N. R., and Dadhwal, V. K.: Inter-annual variability and climate control of terrestrial net primary productivity over India: INTER-ANNUAL VARIABILITY OF TERRESTRIAL NPP OVER INDIA, Int. J. Climatol., 33, 132–142, https://doi.org/10.1002/joc.3414, 2013.

https://doi.org/10.5194/egusphere-2023-817
Preprint. Discussion started: 4 May 2023

Nayak, R. K., Patel, N. R., and Dadhwal, V. K.: Spatio-temporal variability of net ecosystem productivity over India and its relationship to climatic variables, Environ. Earth Sci., 74, 1743–1753, https://doi.org/10.1007/s12665-015-4182-4, 2015.

Parazoo, N. C., Arneth, A., Pugh, T. A. M., Smith, B., Steiner, N., Luus, K., Commane, R., Benmergui, J., Stofferahn, E., Liu, J., Rödenbeck, C., Kawa, R., Euskirchen, E., Zona, D., Arndt, K., Oechel, W., and Miller, C.: Spring photosynthetic onset and net CO_2 uptake in Alaska triggered by landscape thawing, Glob. Change Biol., 24, 3416–3435, https://doi.org/10.1111/gcb.14283, 2018.

Patra, P. K., Niwa, Y., Schuck, T. J., Brenninkmeijer, C. A. M., Machida, T., Matsueda, H., and Sawa, Y.: Carbon balance of South Asia constrained by passenger aircraft CO2 measurements, Atmospheric Chem. Phys., 11, 4163–4175, https://doi.org/10.5194/acp-11-4163-2011, 2011.

Patra, P. K., Canadell, J. G., Houghton, R. A., Piao, S. L., Oh, N.-H., Ciais, P., Manjunath, K. R., Chhabra, A., Wang, T., Bhattacharya, T., Bousquet, P., Hartman, J., Ito, A., Mayorga, E., Niwa, Y., Raymond, P. A., Sarma, V. V. S. S., and Lasco, R.: The carbon budget of South Asia, Biogeosciences, 10, 513–527, https://doi.org/10.5194/bg-10-513-2013, 2013.

Peters, W., Jacobson, A. R., Sweeney, C., Andrews, A. E., Conway, T. J., Masarie, K., Miller, J. B., Bruhwiler, L. M. P., Petron, G., Hirsch, A. I., Worthy, D. E. J., van der Werf, G. R., Randerson, J. T., Wennberg, P. O., Krol, M. C., and Tans, P. P.: An atmospheric perspective on North American carbon dioxide exchange: CarbonTracker, Proc. Natl. Acad. Sci., 104, 18925–18930, https://doi.org/10.1073/pnas.0708986104, 2007.

Peylin, P., Law, R. M., Gurney, K. R., Chevallier, F., Jacobson, A. R., Maki, T., Niwa, Y., Patra, P. K., Peters, W., Rayner, P. J., Rödenbeck, C., van der Laan-Luijkx, I. T., and Zhang, X.: Global atmospheric carbon budget: results from an ensemble of atmospheric

https://doi.org/10.5194/egusphere-2023-817
Preprint. Discussion started: 4 May 2023

CO₂ inversions, Biogeosciences, 10, 6699–6720, https://doi.org/10.5194/bg-10-6699-2013, 2013.

Qiu, R., Han, G., Ma, X., Xu, H., Shi, T., and Zhang, M.: A Comparison of OCO-2 SIF, MODIS GPP, and GOSIF Data from Gross Primary Production (GPP) Estimation and Seasonal Cycles in North America, Remote Sens., 12, 258, https://doi.org/10.3390/rs12020258, 2020.

Rao, A. S., Bala, G., Ravindranath, N. H., and Nemani, R.: Multi-model assessment of trends, variability and drivers of terrestrial carbon uptake in India, J. Earth Syst. Sci., 128, 99, https://doi.org/10.1007/s12040-019-1120-y, 2019.

Rayner, P. J., Enting, I. G., Francey, R. J., and Langenfelds, R.: Reconstructing the recent carbon cycle from atmospheric CO_2, $\delta^{13}C$ and O_2/N_2 observations, Tellus B Chem. Phys. Meteorol., 51, 213–232, https://doi.org/10.3402/tellusb.v51i2.16273, 1999.

Reick, C. H., Raddatz, T., Brovkin, V., and Gayler, V.: Representation of natural and anthropogenic land cover change in MPI-ESM: Land Cover in MPI-ESM, J. Adv. Model. Earth Syst., 5, 459–482, https://doi.org/10.1002/jame.20022, 2013.

Rodda, S. R., Thumaty, K. C., Praveen, M., Jha, C. S., and Dadhwal, V. K.: Multi-year eddy covariance measurements of net ecosystem exchange in tropical dry deciduous forest of India, Agric. For. Meteorol., 301–302, 108351, https://doi.org/10.1016/j.agrformet.2021.108351, 2021.

Rodgers, C. D.: Inverse methods for atmospheric sounding: theory and practice, World Scientific, Singapore, 2000.

Sarma, D., Burman, P. K. D., Chakraborty, S., Gogoi, N., Bora, A., Metya, A., Datye, A., Murkute, C., and Karipot, A.: Quantifying the net ecosystem exchange at a semi-deciduous forest in northeast India from intra-seasonal to the seasonal time scale, Agric. For. Meteorol., 314, 108786, https://doi.org/10.1016/j.agrformet.2021.108786, 2022.

https://doi.org/10.5194/egusphere-2023-817
Preprint. Discussion started: 4 May 2023

Shekhar, A., Buchmann, N., and Gharun, M.: How well do recently reconstructed solar-induced fluorescence datasets model gross primary productivity?, Remote Sens. Environ., 283, 113282, https://doi.org/10.1016/j.rse.2022.113282, 2022.

Sitch, S., Smith, B., Prentice, I. C., Arneth, A., Bondeau, A., Cramer, W., Kaplan, J. O., Levis, S., Lucht, W., Sykes, M. T., Thonicke, K., and Venevsky, S.: Evaluation of ecosystem dynamics, plant geography and terrestrial carbon cycling in the LPJ dynamic global vegetation model: LPJ DYNAMIC GLOBAL VEGETATION MODEL, Glob. Change Biol., 9, 161–185, https://doi.org/10.1046/j.1365-2486.2003.00569.x, 2003.

Sitch, S., Huntingford, C., Gedney, N., Levy, P. E., Lomas, M., Piao, S. L., Betts, R., Ciais, P., Cox, P., Friedlingstein, P., Jones, C. D., Prentice, I. C., and Woodward, F. I.: Evaluation of the terrestrial carbon cycle, future plant geography and climate-carbon cycle feedbacks using five Dynamic Global Vegetation Models (DGVMs): UNCERTAINTY IN LAND CARBON CYCLE FEEDBACKS, Glob. Change Biol., 14, 2015–2039, https://doi.org/10.1111/j.1365-2486.2008.01626.x, 2008.

Sitch, S., Friedlingstein, P., Gruber, N., Jones, S. D., Murray-Tortarolo, G., Ahlström, A., Doney, S. C., Graven, H., Heinze, C., Huntingford, C., Levis, S., Levy, P. E., Lomas, M., Poulter, B., Viovy, N., Zaehle, S., Zeng, N., Arneth, A., Bonan, G., Bopp, L., Canadell, J. G., Chevallier, F., Ciais, P., Ellis, R., Gloor, M., Peylin, P., Piao, S. L., Le Quéré, C., Smith, B., Zhu, Z., and Myneni, R.: Recent trends and drivers of regional sources and sinks of carbon dioxide, Biogeosciences, 12, 653–679, https://doi.org/10.5194/bg-12-653-2015, 2015.

Smith, W. K., Biederman, J. A., Scott, R. L., Moore, D. J. P., He, M., Kimball, J. S., Yan, D., Hudson, A., Barnes, M. L., MacBean, N., Fox, A. M., and Litvak, M. E.: Chlorophyll Fluorescence Better Captures Seasonal and Interannual Gross Primary Productivity Dynamics

https://doi.org/10.5194/egusphere-2023-817
Preprint. Discussion started: 4 May 2023

Across Dryland Ecosystems of Southwestern North America, Geophys. Res. Lett., 45, 748–757, https://doi.org/10.1002/2017GL075922, 2018.

Spahni, R., Joos, F., Stocker, B. D., Steinacher, M., and Yu, Z. C.: Transient simulations of the carbon and nitrogen dynamics in northern peatlands: from the Last Glacial Maximum to the 21st century, Clim. Past, 9, 1287–1308, https://doi.org/10.5194/cp-9-1287-2013, 2013.

Stocker, B. D., Roth, R., Joos, F., Spahni, R., Steinacher, M., Zaehle, S., Bouwman, L., Xu-Ri, and Prentice, I. C.: Multiple greenhouse-gas feedbacks from the land biosphere under future climate change scenarios, Nat. Clim. Change, 3, 666–672, https://doi.org/10.1038/nclimate1864, 2013.

Sun, Y., Frankenberg, C., Wood, J. D., Schimel, D. S., Jung, M., Guanter, L., Drewry, D. T., Verma, M., Porcar-Castell, A., Griffis, T. J., Gu, L., Magney, T. S., Köhler, P., Evans, B., and Yuen, K.: OCO-2 advances photosynthesis observation from space via solar-induced chlorophyll fluorescence, Science, 358, eaam5747, https://doi.org/10.1126/science.aam5747, 2017.

Sun, Y., Frankenberg, C., Jung, M., Joiner, J., Guanter, L., Köhler, P., and Magney, T.: Overview of Solar-Induced chlorophyll Fluorescence (SIF) from the Orbiting Carbon Observatory-2: Retrieval, cross-mission comparison, and global monitoring for GPP, Remote Sens. Environ., 209, 808–823, https://doi.org/10.1016/j.rse.2018.02.016, 2018.

Taylor, T. E., Eldering, A., Merrelli, A., Kiel, M., Somkuti, P., Cheng, C., Rosenberg, R., Fisher, B., Crisp, D., Basilio, R., Bennett, M., Cervantes, D., Chang, A., Dang, L., Frankenberg, C., Haemmerle, V. R., Keller, G. R., Kurosu, T., Laughner, J. L., Lee, R., Marchetti, Y., Nelson, R. R., O'Dell, C. W., Osterman, G., Pavlick, R., Roehl, C., Schneider, R., Spiers, G., To, C., Wells, C., Wennberg, P. O., Yelamanchili, A., and Yu, S.: OCO-3 early mission operations and initial (vEarly) XCO2 and SIF retrievals, Remote Sens. Environ., 251, 112032, https://doi.org/10.1016/j.rse.2020.112032, 2020.

https://doi.org/10.5194/egusphere-2023-817
Preprint. Discussion started: 4 May 2023

Thilakan, V., Pillai, D., Gerbig, C., Galkowski, M., Ravi, A., and Anna Mathew, T.: Towards monitoring the CO_2 source–sink distribution over India via inverse modelling: quantifying the fine-scale spatiotemporal variability in the atmospheric CO_2 mole fraction, Atmospheric Chem. Phys., 22, 15287–15312, https://doi.org/10.5194/acp-22-15287-2022, 2022.

Thompson, R. L., Patra, P. K., Chevallier, F., Maksyutov, S., Law, R. M., Ziehn, T., van der Laan-Luijkx, I. T., Peters, W., Ganshin, A., Zhuravlev, R., Maki, T., Nakamura, T., Shirai, T., Ishizawa, M., Saeki, T., Machida, T., Poulter, B., Canadell, J. G., and Ciais, P.: Top–down assessment of the Asian carbon budget since the mid 1990s, Nat. Commun., 7, 10724, https://doi.org/10.1038/ncomms10724, 2016.

Tian, H., Chen, G., Lu, C., Xu, X., Hayes, D. J., Ren, W., Pan, S., Huntzinger, D. N., and Wofsy, S. C.: North American terrestrial CO2 uptake largely offset by CH4 and N2O emissions: toward a full accounting of the greenhouse gas budget, Clim. Change, 129, 413–426, https://doi.org/10.1007/s10584-014-1072-9, 2015.

van der Meer, P. J., Jorritsma, I. T. M., and Kramer, K.: Assessing climate change effects on long-term forest development: adjusting growth, phenology, and seed production in a gap model, For. Ecol. Manag., 162, 39–52, https://doi.org/10.1016/S0378-1127(02)00049-X, 2002.

Wood, J. D., Griffis, T. J., Baker, J. M., Frankenberg, C., Verma, M., and Yuen, K.: Multiscale analyses of solar-induced florescence and gross primary production, Geophys. Res. Lett., 44, 533–541, https://doi.org/10.1002/2016GL070775, 2017.

Woodward, F. I., Smith, T. M., and Emanuel, W. R.: A global land primary productivity and phytogeography model, Glob. Biogeochem. Cycles, 9, 471–490, https://doi.org/10.1029/95GB02432, 1995.

Wu, G., Guan, K., Jiang, C., Kimm, H., Miao, G., Bernacchi, C. J., Moore, C. E., Ainsworth, E. A., Yang, X., Berry, J. A., Frankenberg, C., and Chen, M.: Attributing differences of solar-

https://doi.org/10.5194/egusphere-2023-817
Preprint. Discussion started: 4 May 2023

induced chlorophyll fluorescence (SIF)-gross primary production (GPP) relationships between two C4 crops: corn and miscanthus, Agric. For. Meteorol., 323, 109046, https://doi.org/10.1016/j.agrformet.2022.109046, 2022.

Yu, G.-R., Zhu, X.-J., Fu, Y.-L., He, H.-L., Wang, Q.-F., Wen, X.-F., Li, X.-R., Zhang, L.-M., Zhang, L., Su, W., Li, S.-G., Sun, X.-M., Zhang, Y.-P., Zhang, J.-H., Yan, J.-H., Wang, H.-M., Zhou, G.-S., Jia, B.-R., Xiang, W.-H., Li, Y.-N., Zhao, L., Wang, Y.-F., Shi, P.-L., Chen, S.-P., Xin, X.-P., Zhao, F.-H., Wang, Y.-Y., and Tong, C.-L.: Spatial patterns and climate drivers of carbon fluxes in terrestrial ecosystems of China, Glob. Change Biol., 19, 798–810, https://doi.org/10.1111/gcb.12079, 2013.

Yu, L., Wen, J., Chang, C. Y., Frankenberg, C., and Sun, Y.: High-Resolution Global Contiguous SIF of OCO-2, Geophys. Res. Lett., 46, 1449–1458, https://doi.org/10.1029/2018GL081109, 2019.

Zaehle, S. and Friend, A. D.: Carbon and nitrogen cycle dynamics in the O-CN land surface model: 1. Model description, site-scale evaluation, and sensitivity to parameter estimates: SITE-SCALE EVALUATION OF A C-N MODEL, Glob. Biogeochem. Cycles, 24, n/a-n/a, https://doi.org/10.1029/2009GB003521, 2010.

Zeng, Jiye: A Data-driven Upscale Product of Global Gross Primary Production, Net Ecosystem Exchange and Ecosystem Respiration (ver.2020.2), https://doi.org/10.17595/20200227.001, 2020.

Zhang, Y., Yu, Q., Jiang, J., and Tang, Y.: Calibration of Terra/MODIS gross primary production over an irrigated cropland on the North China Plain and an alpine meadow on the Tibetan Plateau: CALIBRATION OF TERRA/MODIS GROSS PRIMARY PRODUCTION, Glob. Change Biol., 14, 757–767, https://doi.org/10.1111/j.1365-2486.2008.01538.x, 2008.

https://doi.org/10.5194/egusphere-2023-817
Preprint. Discussion started: 4 May 2023

Zhang, Y., Guanter, L., Berry, J. A., van der Tol, C., Yang, X., Tang, J., and Zhang, F.: Model-based analysis of the relationship between sun-induced chlorophyll fluorescence and gross primary production for remote sensing applications, Remote Sens. Environ., 187, 145–155, https://doi.org/10.1016/j.rse.2016.10.016, 2016.